REPORT DOCUMENTATION PAGE

Form Approved OMB NO. 0704-0188

1. REPORT DATE (DD-MM-YYYY)	2. REPORT TYPE	3. DATES COVERED (From - To)
10-08-2015	Final Report	11-May-2011 - 10-May-2015

4. TITLE AND SUBTITLE

Final Report: Investigation of Multi-Functional Ferroelectric Nanorod/Carbon Nanotube/Polymer Composites and Shape Memory Alloy Treatment for Vibration Control of Fire Control System to Improve Firing Accuracy

5a. CONTRACT NUMBER
W911NF-11-1-0131

5b. GRANT NUMBER

5c. PROGRAM ELEMENT NUMBER
206022

6. AUTHORS
Cesar Levy

5d. PROJECT NUMBER

5e. TASK NUMBER

5f. WORK UNIT NUMBER

7. PERFORMING ORGANIZATION NAMES AND ADDRESSES
Florida International University
11200 SW 8th St
MARC 430
Miami, FL 33199 -0001

8. PERFORMING ORGANIZATION REPORT NUMBER

9. SPONSORING/MONITORING AGENCY NAME(S) AND ADDRESS (ES)
U.S. Army Research Office
P.O. Box 12211
Research Triangle Park, NC 27709-2211

10. SPONSOR/MONITOR'S ACRONYM(S)
ARO

11. SPONSOR/MONITOR'S REPORT NUMBER(S)
58940-EG-REP.22

12. DISTRIBUTION AVAILIBILITY STATEMENT
Approved for Public Release; Distribution Unlimited

13. SUPPLEMENTARY NOTES
The views, opinions and/or findings contained in this report are those of the author(s) and should not contrued as an official Department of the Army position, policy or decision, unless so designated by other documentation.

14. ABSTRACT

We have created and tested several sensors: one is PANI/MWCNT composite; a second was a polyurethane/Buckypaper composite and a third was a MWCNT/DYAD/MWCNT composite. The first sensor was a continuation of the research work we have carried on in the past 2 years. The second was a decision to see if the polyurethane can be used to modify the Buckypaper sensor we had investigated in our previous ARO grant. The third was an outcome of the results that we had obtained from the other two sensors. In our 2013-14 progress report we had reported on the preparation and characterization of the polyaniline/MWCNT (PANI/MWCNT) and

15. SUBJECT TERMS
PU/Buckypaper sensor, PANI/MWCNT sensor, loss factor, Dynamic Sensing, Strain Sensing

16. SECURITY CLASSIFICATION OF:			17. LIMITATION OF ABSTRACT	15. NUMBER OF PAGES	19a. NAME OF RESPONSIBLE PERSON
a. REPORT	b. ABSTRACT	c. THIS PAGE			Cesar Levy
UU	UU	UU	UU		19b. TELEPHONE NUMBER 305-348-3643

Report Title

Final Report: Investigation of Multi-Functional Ferroelectric Nanorod/Carbon Nanotube/Polymer Composites and Shape Memory Alloy Treatment for Vibration Control of Fire Control System to Improve Firing Accuracy

ABSTRACT

We have created and tested several sensors: one is PANI/MWCNT composite; a second was a polyurethane/Buckypaper composite and a third was a MWCNT/DYAD/MWCNT composite. The first sensor was a continuation of the research work we have carried on in the past 2 years. The second was a decision to see if the polyurethane can be used to modify the Buckypaper sensor we had investigated in our previous ARO grant. The third was an outcome of the results that we had obtained from the other two sensors. In our 2013-14 progress report we had reported on the preparation and characterization of the polyaniline/MWCNT (PANI/MWCNT) and Polyurethane/ZnO/MWCNT (PU/ZnO/MWCNT nanocomposite films. Also discussed in the report were the vibration aspects that needed to be addressed, namely cantilever beam vibrations that were representative of the main barrel of a tank or structural health monitoring, for example. We have been working on determining the proper shape of the sensor and its placement in order to achieve the goals of the grant, namely to maintain a sensor that has linear properties with applied load yet introduce more damping into the sensor than previously existed with the MWCNT buckypaper. Though the grant ended in May, 2015, we plan to continue to work on the control aspect, and, if allowed, we plan to report results to ARO.

Enter List of papers submitted or published that acknowledge ARO support from the start of the project to the date of this printing. List the papers, including journal references, in the following categories:

(a) Papers published in peer-reviewed journals (N/A for none)

Received	Paper
08/07/2015 14.00	Hadi Fekrmandi, Javier Rojas, Jason Campbell, Ibrahim Nur Tansel, Bulent Kaya, Sezai Taskin. Inspection of the Integrity of a Multi-Bolt Robotic Arm Using a Scanning Laser Vibrometer and Implementing the Surface Response to Excitation Method (SuRE), International Journal of Prognostics and Health Management, (01 2014): 1. doi:
08/07/2015 12.00	Javier Rojas, Ibrahim N. Tansel, Ahmet Yapici, Balemir Uragun, Hadi Fekrmandi. Investigation of the computational efficiency and validity of the surface response to excitation method, measurement, (02 2015): 0. doi: 10.1016/j.measurement.2014.10.053
08/07/2015 11.00	Muhammad Unal, Hadi Fekrmandi, Amin Baghalian, Shervin Tashakori, Kathleen Oyola, Abdullah Alsenawi, Ibrahim Nur Tansel. A non-contact method for part-based process performance monitoring in end milling operations, The International Journal of Advanced Manufacturing Technology, (07 2015): 0. doi: 10.1007/s00170-015-7523-2
08/07/2015 13.00	Weiwei LIN,, Xiangxing KONG, Cesar LEVY. Preparation of Polyaniline Multi-wall Carbon NanotubesNanocomposites Films/Discs and Characterizationof their Electrical, Mechanical and Damping Properties, Sensors and Transducers, (04 2015): 129. doi:
08/25/2014 4.00	Tomislav Kosta, Igor Tsukanov. Meshfree Modeling of Dynamic Response of Mechanical Structures, Meccanica, (01 2014): 2399. doi:
TOTAL:	**5**

Number of Papers published in peer-reviewed journals:

(b) Papers published in non-peer-reviewed journals (N/A for none)

Received		Paper
08/25/2014	3.00	Tomislav Kosta, Igor Tsukanov. 3D Natural Vibration Analysis with Meshfree Solution Structure Method, Journal of Vibration and Acoustics, (05 2014): 51011. doi:
08/25/2014	6.00	H. Fekrmandi, J. Rojas, , J. Campbell,, I. N. Tansel, , B. Kaya, , S. Taskin. Inspection of the Integrity of a Multi-Bolt Robotic Arm Using a Scanning Laser Vibrometer and Implementing the Surface Response to Excitation Method (SuRE), International Journal of Prognostics and Health Management, (01 2014): 1. doi:
TOTAL:		**2**

Number of Papers published in non peer-reviewed journals:

(c) Presentations

Two presentations, one a presentation and poster session, the other a poster session only
4th International Conference and Exhibition on Materials Science & Engineering September 14-16, 2015 Orlando, Florida, USA: Preparation of Polyurethane/Buckypaper composites films and characterization of their Structural Vibration Damping and Strain Sensing Properties, Weiwei LIN, Yonatan ROTENBERG, Hadi FEKRMAND, Kevin P. WARD, Cesar LEVY, Florida International University (presentation and poster session)

The 5th Annual World Congress of Nano Science & Technology-2015 (Nano S&T-2015), Xi'an, China, September 24-26:Preparation of Buckypaper/DYAD/Polyaniline/MWCNT composites films and characterization of their Structural Vibration Damping, Weiwei LIN, Yonatan ROTENBERG, Hadi FEKRMAND, Kevin P. WARD, Cesar LEVY, Florida International University (poster session)

Number of Presentations: 2.00

Non Peer-Reviewed Conference Proceeding publications (other than abstracts):

Received		Paper
08/25/2014	8.00	H. Fekrmandi, , G. Ramanathan, , I. N. Tansel. Automation of manufacturing process monitoring for CNC milling machines using a remote sensing method based on high–frequency surface guided waves, 27th Florida Conference on Recent Advances in Robotics, FCRAR 2014. 02-MAY-14, . : ,
08/30/2013	2.00	Hadi Fekrmandi, Javier Rojas, Ibrahim N. Tansel, Balemir Uragun, Sergio Gonzalez. IMPLEMENTING THE SURFACE RESPONSE TO EXCITATION METHOD (SuRE) WITH NON-CONTACT SENSOR AT HARD TO REACH LOCATIONS, IWSHM 2013. 10-SEP-13, . : ,
TOTAL:		**2**

Number of Non Peer-Reviewed Conference Proceeding publications (other than abstracts):

Peer-Reviewed Conference Proceeding publications (other than abstracts):

Received	Paper	
08/07/2015	20.00	Danilo Delgado,, Michael Fisher, , Lucia Melara, , Melissa Morris, , Sabri Tosunoglu. SWAT Bot and its Future Use as aStrategic Response Robot, 2015 Florida Conference on Recent Advances in Robotics. 14-MAY-15, . : ,
08/07/2015	15.00	Hadi Fekrmandi, Ibrahim N. Tansel, Abdullah Alrashidi, David Meiller. LASER SCANNING VIBROMETER FOR REMOTE PROCESS PERFORMANCEMONITORING OF AUTOMATED MANUFACTURING OPERATIONS, Early Career Technical Conference 2014. 01-NOV-14, . : ,
08/07/2015	17.00	Jonathan Hipps,, Alejandro Osorio, , Gianfranco Pisani,, Sebastian Rojas, , Melissa Morris, , Sabri Tosunoglu. Laser Eye Surgery Robot, 2015 Florida Conference on Recent Advances in Robotics. 14-MAY-15, . : ,
08/07/2015	16.00	Hadi Fekrmandi, Gurunath Ramanathan, Ibrahim Nur Tansel. Automation of manufacturing process monitoring for CNCmilling machines using a remote sensing method basedon high–frequency surface guided waves, 2014 Florida Conference on Recent Advances in Robotics. 08-MAY-14, . : ,
08/07/2015	19.00	Melissa Morris, Sabri Tosunoglu. Robotic Ocular Surgery, 2015 Florida Conference on Recent Advances in Robotics. 14-MAY-15, . : ,
08/07/2015	18.00	Alexis Garo,, Lucia Melara, , Robert Scott, , Melissa Morris, , Sabri Tosunoglu. Natural Gait Inducing Transtibial Prosthetic, 2015 Florida Conference on Recent Advances in Robotics. 14-MAY-15, . : ,
08/25/2014	7.00	H. Fekrmandi, , J. Rojas, , M. Wolff, , I. N. Tansel, , S. Gonzalez, , B. Uragun. Monitoring The Health of a Beam Remotely by Using Scanning Laser Vibrometer, ASME Early Career Technical Conference Proceedings, ECTC 2013. 01-NOV-13, . : ,

TOTAL: **7**

Number of Peer-Reviewed Conference Proceeding publications (other than abstracts):

(d) Manuscripts

Received		Paper
08/07/2015	21.00	Weiwei LIN, , Yonatan ROTENBERG,, Hadi FEKRMANDI, , Kevin P. WARD, , Cesar LEVY. Multifunctional Materials of Polyurethane/MWCNT and Evaluation ofDamping and Displacement Sensing Properties, Journal of Nanomaterials (07 2015)
08/25/2014	5.00	H Fekrmandi, I Tansel, R Kiflemariam. Laser scanning vibrometer for remote process performance monitoring of automated manufacturing operations, SUBMITTED TO the 2014 ASME IMECE conference (11 2014)
08/25/2014	9.00	H. Fekrmandi, , J. Rojas, , I. N. Tansel, , A. Yapici, , B. Uragun. Study of the Computational Efficiency and Validity of the Surface Response to Excitation Method, measurement (05 2014)
08/30/2013	1.00	Andy Nieto, Debrupa Lahiri, Arvind Agarwal. Nano Dynamic Mechanical Behavior of Graphene NanoPlatelets Reinforced Tantalum Carbide, Scripta Materialia (06 2013)
TOTAL:		**4**

Number of Manuscripts:

Books

Received		Book
TOTAL:		

Received	Book Chapter

TOTAL:

Patents Submitted

Patents Awarded

Awards

none

Graduate Students

NAME	PERCENT_SUPPORTED	Discipline
Morris, Melissa	1.00	
Bamgebade, Ayobami	1.00	
FTE Equivalent:	**2.00**	
Total Number:	**2**	

Names of Post Doctorates

NAME	PERCENT_SUPPORTED
FTE Equivalent:	
Total Number:	

Names of Faculty Supported

NAME	PERCENT_SUPPORTED	National Academy Member
Cesar Levy	0.03	
FTE Equivalent:	**0.03**	
Total Number:	**1**	

Names of Under Graduate students supported

NAME	PERCENT_SUPPORTED	Discipline
Rotenberg, Yonatan	1.00	Mechanical Engineering
Ward-Jimenez, Kevin	0.01	Mechanical Engineering
FTE Equivalent:	**1.01**	
Total Number:	**2**	

Student Metrics

This section only applies to graduating undergraduates supported by this agreement in this reporting period

The number of undergraduates funded by this agreement who graduated during this period:	1.00
The number of undergraduates funded by this agreement who graduated during this period with a degree in science, mathematics, engineering, or technology fields:.....	1.00
The number of undergraduates funded by your agreement who graduated during this period and will continue to pursue a graduate or Ph.D. degree in science, mathematics, engineering, or technology fields:.....	1.00
Number of graduating undergraduates who achieved a 3.5 GPA to 4.0 (4.0 max scale):.....	1.00
Number of graduating undergraduates funded by a DoD funded Center of Excellence grant for Education, Research and Engineering:.....	0.00
The number of undergraduates funded by your agreement who graduated during this period and intend to work for the Department of Defense	0.00
The number of undergraduates funded by your agreement who graduated during this period and will receive scholarships or fellowships for further studies in science, mathematics, engineering or technology fields:	0.00

Names of Personnel receiving masters degrees

NAME
Total Number:

Names of personnel receiving PHDs

NAME
Total Number:

Names of other research staff

NAME	PERCENT_SUPPORTED
FTE Equivalent:	
Total Number:	

Sub Contractors (DD882)

Inventions (DD882)

Scientific Progress

see attachment

Technology Transfer

none

Final Progress Report for Proposal Number: 58940-EG-REP
Agreement Number: W911NF-11-1-0131
Due on August 10, 2015
for the period beginning August 1, 2014 and ending May 10, 2015.

Principal Investigator: Dr. Cesar Levy, Florida International University
Post Doctoral Research Associate: None

Table of Contents

Final Progress Report for Proposal Number: 58940-EG-REP
Agreement Number: W911NF-11-1-0131
Due on August 10, 2015
for the period beginning August 1, 2014 and ending May 10, 2015.

Principal Investigator: Dr. Cesar Levy, Florida International University
Post-Doctoral Research Associate: none

Summary of the Progress Made for this Proposal

During this period, we created several sensors. We then tested the created sensor for electric conducting properties necessary to measure extension through the change in voltage. We also had to evaluate some of its material properties to insure that it had damping qualities as well as stability over a usable range of temperatures. We successfully synthesized different viscoelastic polyurethanes (PU). We also synthesized other piezoelectric materials. We also produced different component films such as MWCNT/PU and PANI/PU for evaluation to include different width of the sensors and different coverage percentage of sensor over aluminum base beams, and evaluated sensor placement vis-à-vis sensor damping. Damping properties and strain sensor properties were characterized by those samples. To date, we have created sensors in disc form and in rectangular form but have opted to continue with the rectangular form of the sensor. We also used the laser vibrometer in the testing phase to determine the damping characteristics of the sensor, the drift and dynamic sensing of the sensor, as well.

Technical Objectives of the Proposal

The objective of the proposal is to investigate the feasibility and placement location of applying piezoelectric ceramic nanorod/multi-walled nanotube (MWCNT) and polymer composite viscoelastic films/patches as sensors and damping treatment in conjunction with SMA materials as actuators for vibration and noise attenuation. To reach our final technical objectives, we plan to carry out the following detailed research steps within three years:

- Fabrication and component optimization of piezoelectric ceramic nanorod / MWCNT /polymer composites.
- Dynamic damping property investigation of the piezoelectric ceramic nanorod / MWCNT /polymer composites.
- Static and dynamic sensing property investigation of the ferroelectric ceramic whisker/ MWCNT/ polymer composites
- Application of ferroelectric ceramic whisker/MWCNT/Polymer with SMA to the beam structure.

Time Frame as listed in the proposal

This was originally a 3-year (36-month) proposal. Because of a problem with getting the

equipment to do the sensor synthesis in the second year, we had to redefine our goals for the third and fourth years and also to request a no-cost extension to work on the completion of the goals of project. We have been working on determining the proper shape of the sensor and its placement in order to achieve the goals of the grant, namely to maintain a sensor that has linear properties with applied load yet introduce more damping into the sensor than previously existed with the MWCNT buckypaper. Though the grant ended in May, 2015, we plan to continue to work on the control aspect, and, if allowed, we plan to report results to ARO.

We have created and tested several sensors: one is PANI/MWCNT composite; a second was a polyurethane/Buckypaper composite and a third was a MWCNT/DYAD/MWCNT composite. The first sensor was a continuation of the research work we have carried on in the past 2 years. The second was a decision to see if the polyurethane can be used to modify the Buckypaper sensor we had investigated in our previous ARO grant. The third was an outcome of the results that we had obtained from the other two sensors. In our 2013-14 progress report we had reported on the preparation and characterization of the polyaniline/MWCNT (PANI/MWCNT) and Polyurethane/ZnO/MWCNT (PU/ZnO/MWCNT nanocomposite films. Also discussed in the report were the vibration aspects that needed to be addressed, namely cantilever beam vibrations that were representative of the main barrel of a tank or structural health monitoring, for example.

Carbon nanotubes are considered to be the ultimate low-density high-modulus fibers [1]. Our previous results also indicated that MWCNT films are capable of being strain sensors [2]. The static test results showed a clear, repeatable, stable and temperature independent linear relationship between the voltage output from the Wheatstone bridge and the applied strain. The dynamic test with different loading frequencies also indicated that the MWCNT film sensor is more sensitive than the conventional foil strain gage in the higher frequency range, which would be a great advantage for structural health monitoring application. In a previous ARO grant we had found that Buckypaper sensors had characteristic damping ratios which were quite small, on the order of 0.006-0.007 and published same in [3].

In the first paper published in Sensors and Transducers, titled “Preparation of polyaniline multi-wall carbon nanotubes nanocomposites films/discs and characterization of their electrical, mechanical and damping properties” [4], the information provided in the previous progress report was the basis for the paper. Therein we reported the process by which the PANI/MWCNT was made using a frit compression technique; the morphological characterization of the PANI/MWCNT film; its electrical resistance as a function of % MWCNT; its mechanical properties via a nanoindentation test; its thermal stability characteristics; some preliminary data on the vibration damping ability of a rectangular sensor; how that damping ability of the sensor depended on the thickness of the beam; whether the beam was clamped on the sensor side or the end furthest from the sensor; whether the beam had the sensor on one side only or both sides; and the damping ratio’s dependence on the % MWCNT in the sensor. This paper is uploaded for your records.

PANI/MWCNT New Findings (to be published)

We concentrate on new results here. The PANI/11%MWCNT composite was created using several different loadings. This was done in order to check on whether the load application to

create the composite, would have any major effect on the damping capability of the composite. We attempted creation of the composite at several pressures-namely 50, 65, 70, 75 and 100 lbs. We concentrated on the PANI/ 11%MWCNT composite as that one was found to provide the best damping ratio. The methodology used for this investigation is given below.

64.375 mg of MWCNT were dispersed by sonication in 125 ml of 1M HCl for 30 min. Then, 1.287 g of aniline was added and the mixture was sonicated for another 30 min. After that, 1.027 g of ammonium persulphate (APS) dissolved in 125 ml of 1 M HCl was added at once and polymerization was conducted at 0 °C with water-ice bath under sonication for 4 hrs. The precipitated products were washed with deionized water. Then the PANI/11% wt MWCNT composite was made.

454.54 mg of obtained PANI/11% wt MWCNT suspension was transferred into a specially built 50 ml cuboid mold (see **Figure 1**), which was equipped with frits with a pore diameter of 70 µm (frits purchased from Sigma-Aldrich). In order to remove the solvent, five different compression forces of were applied to the plungers, of which we show two, which were measured by FlexForce adapter (See **Figure 2**). After the solvent was squeezed out, the frits- PANI/11% wt MWCNT sandwich with the cuboid mold was dried at 110 °C in an oven for 12 hrs. The PANI/11% wt MWCNT composite film was obtained after removing it from the cuboid mold.

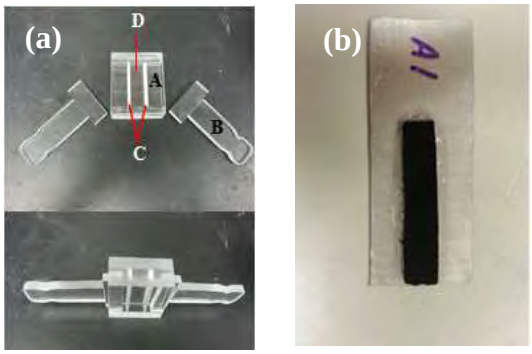

Figure 1. The frit compression system for making PANI/11% wt MWCNT nanocomposite films. (a) The frit compression system, (b) are the photo image of PANI/MWCNT nanocomposites. Inserts are A: cuboid; B: plungers; C: polypropylene frits and D: composites suspension.

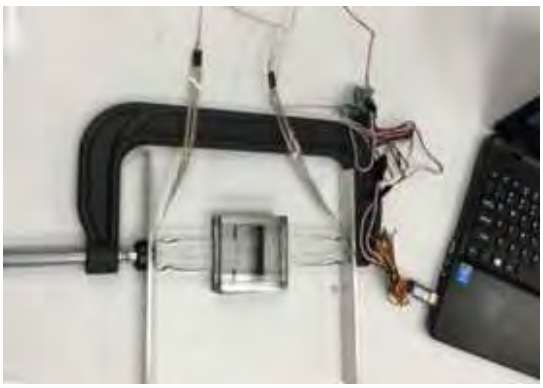

Figure 2. Schematic image of 65 lbs and 75 lbs force applied to plungers measured by FlexiForce adapter.

Figure 3 shows that there is little difference between the two compression force test results.

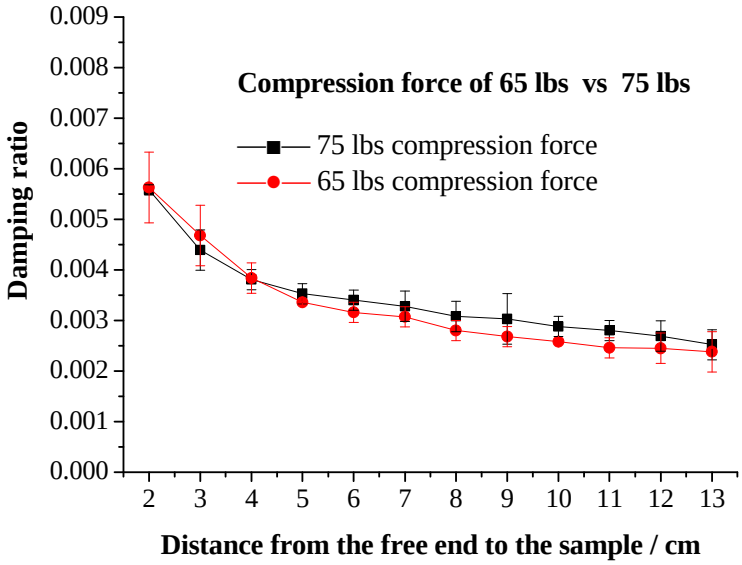

Figure 3. Damping ratios comparison between 65 lbs and 75 lbs compression force of PANI/MWCNT composites when clamped on the free end side. The differences are not statistically significant.

PANI/MWCNT nanocomposites damping test

Single side attachment: Both 65 lbs and 75 lbs applied force of PANI/MWCNT with dimension of 3 cm ×0.9 cm×1.9 mm were attached upon 20.5 cm ×0.9 cm×1.25 mm Aluminum base beam on one side (see Fig. 4) using a thin layer of glue. The specimen was dried at room temperature for 24 hrs. The unclamped side was then made to vibrate and the damping ratio was determined for various lengths of the beam. The sample size did not change. Free vibration comparisons were made by using either the sample side, #, or the uncovered side, *, alternately, as the fixed support for the cantilever beam. The red dashed lines shown in Figure 4 defined the locations where the beam was clamped. The side of the Al base beam that was without the sample was cut then clamped and vibrated. The unclamped side was then made to vibrate and a parameter called the damping ratio was determined. This process was repeated after cutting the beam 1 cm at a time, until the cut end was next to the sample. The damping ratios then were compared.

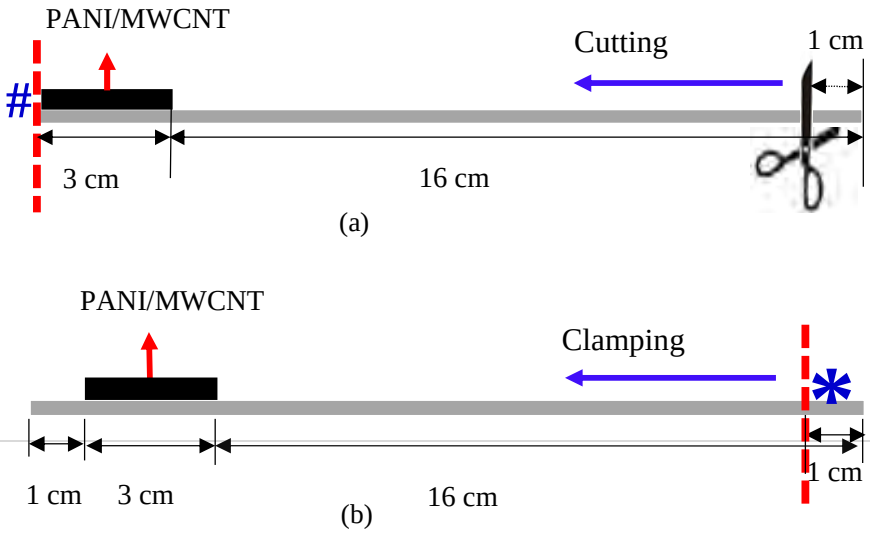

Figure 4. Schematic images of single side's attachment. The dimension of samples, Al beams and the locations where samples were attached, the locations of sample side, #, and free end side, *, where the beam was clamped and also the directions and lengths for both cutting and clamping.

"Sandwich" attachment: The sample used here is with 75 lbs applied force on the PANI/MWCNT composite. All the dimensions of sample and aluminum base beams, the clamped locations and the directions and lengths for both cutting and clamping remained the same. The only change is that the Aluminum beam was "sandwiched" on both sides with the sample (see **Fig. 5**).

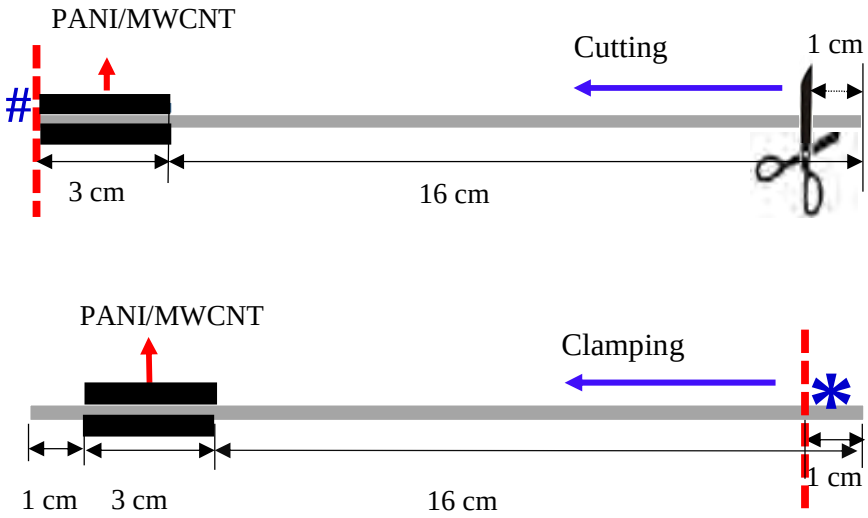

Figure 5. Schematic images of double sides' attachment. The dimension of samples, Al beams and the locations where samples were attached, the locations of sample side, #, and free end side, *, where the beam was clamped and also the directions and lengths for both cutting and clamping.

Damping Test Methodology for PANI/MWCNT

The cantilever beams of **Figures 4** and **5** were given the same small initial displacement and then released for free vibration. Free end displacements were measured by laser vibrometer and a two channels digital oscilloscope displayed and stored the signal. Five trials were made for each setup and the mean value of the damping ratio was calculated. This ratio can be related to the logarithmic decrement of consecutive maxima of end displacements and can be correlated to how much vibration energy is removed by the sample. The higher the damping ratio, the better the sample acts as a damper.

Damping results for single side attachment for PANI/MWCNT

As mentioned previously, the reason for the creation of the composite is for use as a sensor-actuator with damping capabilities. To check on the damping capability aspect, several tests were performed. **Figure 4** is the configuration of the Al base beam single side attachment tests setup. Free vibration trial results are shown in **Fig. 7.**

Five trials were run for each of the clamped locations listed. The results clearly showed that the damping ratio increased as the distance from the free end to the sample decreased for clamping on both the free end side, *, and the sample side, #, (see **Fig. 7,** red and blue data respectively). However, when clamped on the sample side #, damping ratios will decrease as the distance from the free end to the

sample is further decreased. After that, it increases again and reaches the highest damping value of 0.0131.

In most cases, the damping ratios when clamped on the free end side, *, are lower than when clamped on the sample side, #. For example, the highest damping ratios when clamping on free end side, *, is 0.0131, where the distance from sample to the free end is 0 cm. It is the only case for which both clamping conditions (free end side or sample side) are the same. However, when the distance from sample to the free end is 1 cm and clamping is on the free end side,*, the damping ratio is still lower (0.00757) than the damping ratio when clamped on the sample side, #, and the free end is at its furthest (0.00788). Finally, when the sample is symmetric with the ends, the damping ratio values must match.

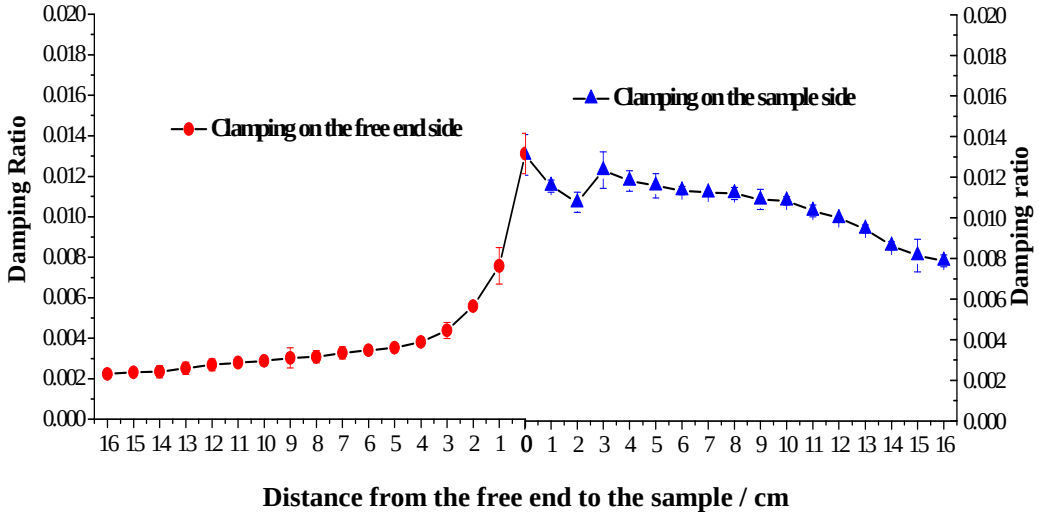

Figure 7. Damping ratios of single side attached PANI/MWCNT clamped on the uncovered side, *, and sample side, #.

Damping results for double sides' attachment for PANI/MWCNT

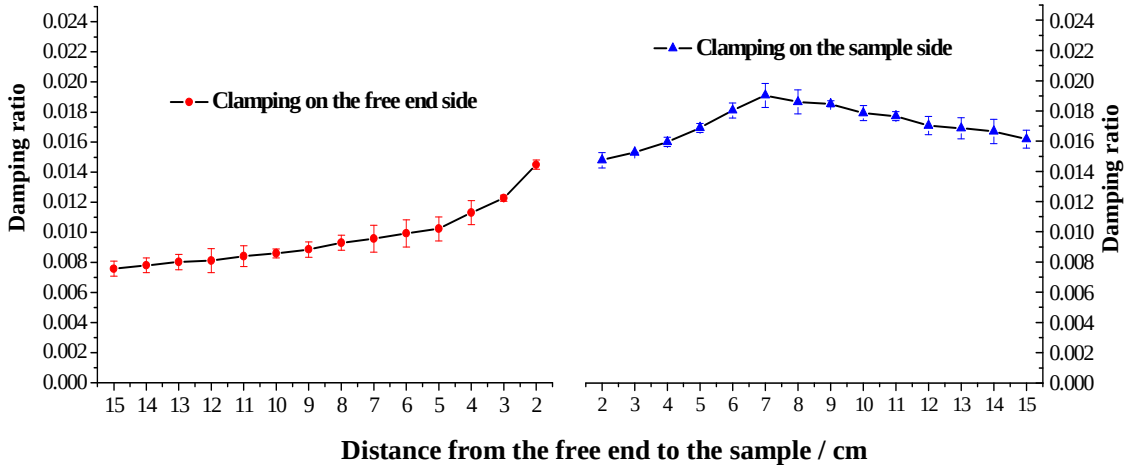

Figure 8. Damping ratios of both sides attached PU/Buckypaper clamped on the uncovered side, *, and sample side, #.

The double sides' attachment test, whose setup is shown in **Fig. 5,** displayed similar type trend as the damping ratios for single sided attachment (See **Fig. 8)**. However, the double sides' attachment has overall higher damping ratios compared with single side attachment. It reached the highest damping ratio of 0.019 with double sides' attachment when the sample is 7 cm away from the free end. This means that there was more uncovered beam when the maximum damping ratio is reached in this setup than in the single side attachment setup, and, that single side attachment requires almost complete beam coverage to achieve the best damping ratio. Also, the damping ratios when the beam is clamped on the sample side, #, is higher than when the beam is clamped on the free end side, *. The values of Y-coordinate is very close at 0 cm of X-coordinate, which is expected. When we compare results to just the buckypaper sensor, the maximum damping ratio is 3 times as large. We note that these trends follow the trends reported for constrained viscoelastic layer damping.

Dynamic Sensing Capability of the PANI/MWCNT

PANI dynamic sensing graphs are provided next. Sensing was accomplished by inputing a known frequency to the beam with sensor via a test bed to which the beam and sensor were attached. The input signal applied was from 10-5000 Hz. Shown here are results of the captured signals up to 1000 Hz.

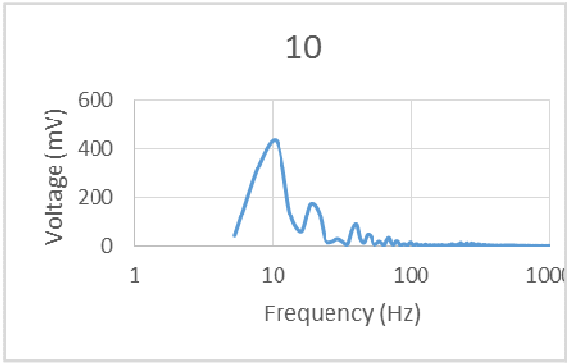

a) 10 Hz – PANI/MWCNT – Magnitude: 428.6999 mV

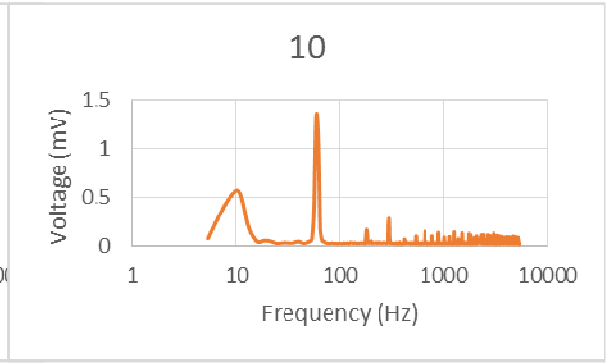

b) 10 Hz – Foil Strain Gage – Magnitude: 0.560121 mV

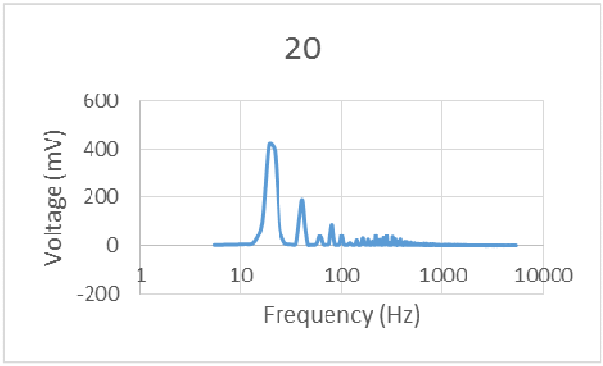

c) 20 Hz – PANI/MWCNT – Magnitude: 418.0301 mV

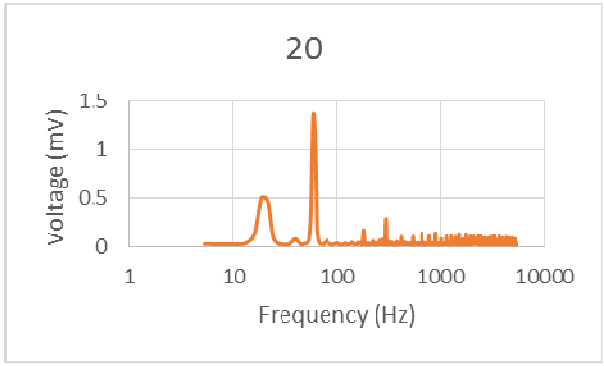

d) 20 Hz – Foil Strain Gage – Magnitude: 0.498347 mV

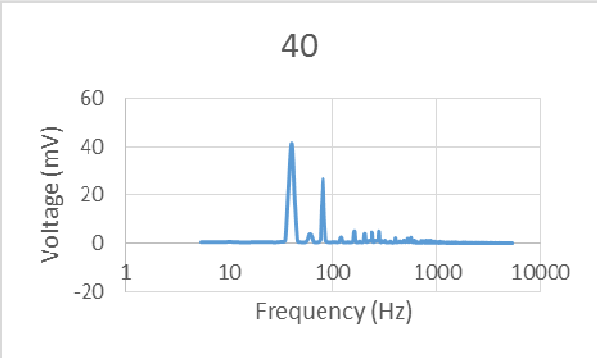

e) 40 Hz – PANI/MWCNT – Magnitude: 41.29593 mV

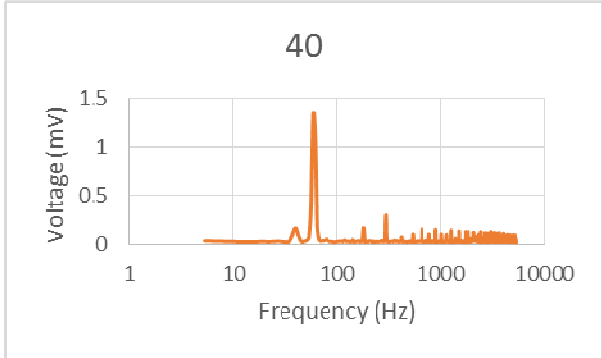

f) 40 Hz – Foil Strain Gage – Magnitude: 0.1627 mV

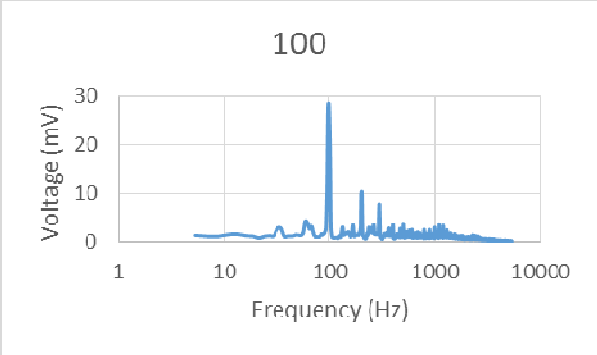

g) 100 Hz – PANI/MWCNT – Magnitude: 28.27814 mV

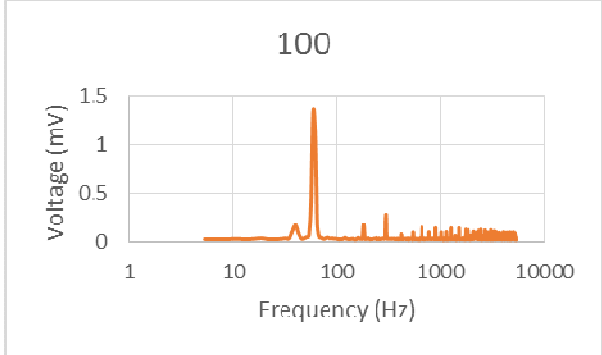

h) 100 Hz – Foil Strain Gage – Magnitude: 0.03146 mV

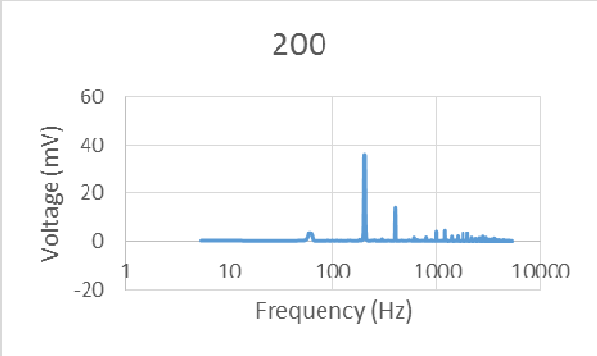

i) 200 Hz – PANI/MWCNT – Magnitude: 35.98084 mV

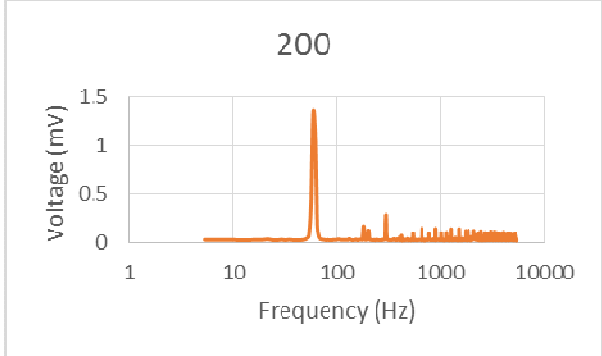

j) 200 Hz – Foil Strain Gage – Magnitude: 0.130066 mV

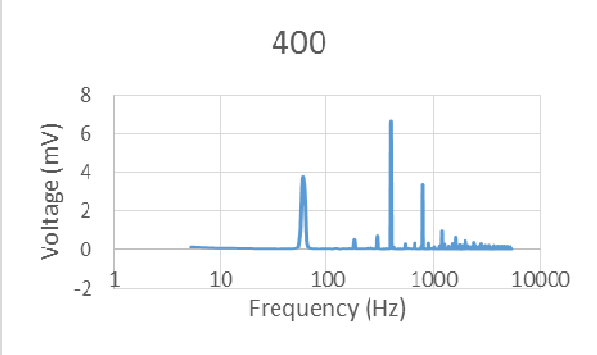

k) 400 Hz – PANI/MWCNT – Magnitude: 6.614911 mV

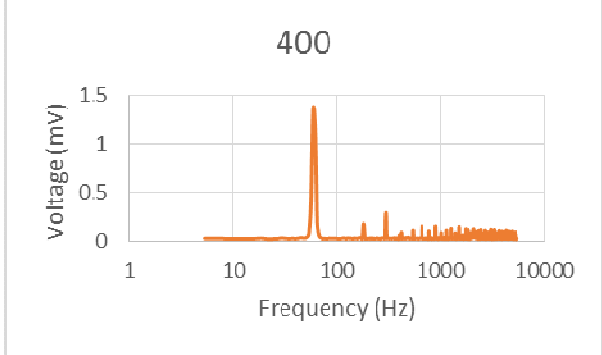

l) 400 Hz – Foil Strain Gage – Magnitude: 0.058299

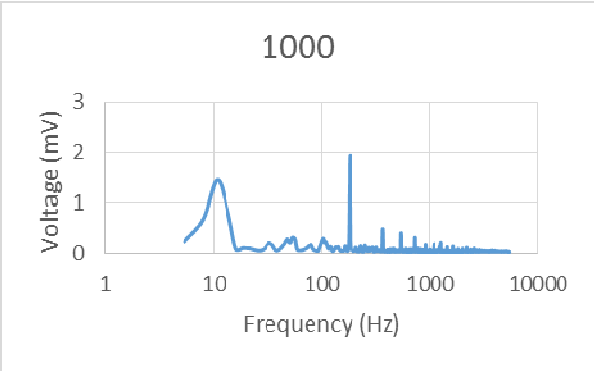

m) 1000 Hz– PANI/MWCNT – Magnitude: 0.0596 mV

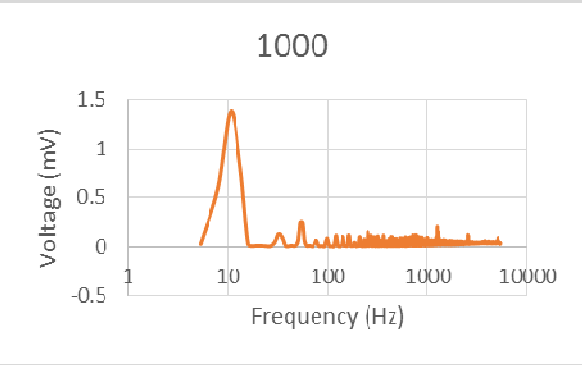

n) 1000 Hz – Foil Strain Gage – Magnitude: 0.06355 mV

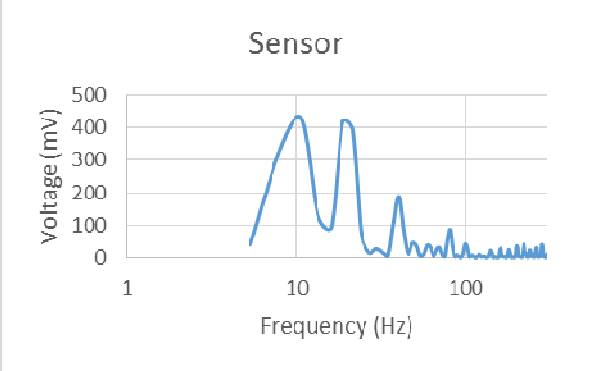

o) FRF – PANI/MWCNT – sensor (10 Hz to 1000 Hz)

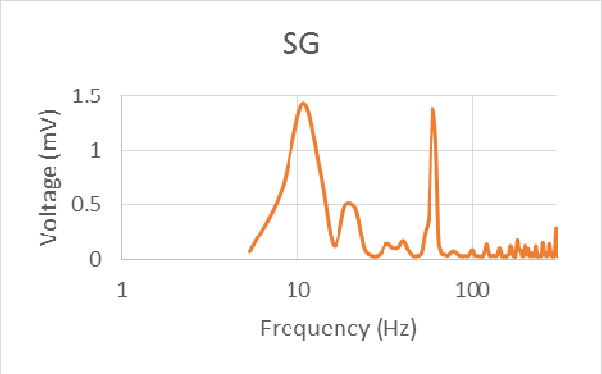

p) FRF – Foil strain gage (10 Hz to 1000 Hz)

Figure 9. Frequency Response Functions of the PANI/MWCNT sensor and foil strain gage for various frequencies (a)-(n). Graphs (o) and (p) represent a superposition of the previous graphs to indicate the superior sensitivity of the PANI/MWCNT in the 10-1000 Hz range.

It is found that the PANI/MWCNT sensor was very much more sensitive than the foil strain gage up until 400 Hz and the signal produced the highest peak in the FRF graphs. Beyond that frequency, either the two produced similar magnitudes or were not the highest peaks distinguishable. The magnitudes listed represents the signal height sensed by the sensor (blue) and the foil strain gage (orange). The last two graphs represent the superposition of the previous graphs to show that the sensor is much more sensitive over a larger range of frequencies.

Static sensing properties for the PANI/MWCNT -The drift effect

The stability of each sensor was tested and typical results for some samples and strain gage are discussed following explanations of the test procedures.

Sample Setup for drift, static tensile test for the PANI/MWCNT

The sensor was bonded to the center of a 61 mil thick 6061-T6 Aluminum rectangular bar using 3M CA100 liquid instant adhesive. Each specimen was held in place by a weight and dried in room temperature for 24 hrs. The bonding area was prepared to ensure a smooth surface, as is normally

defined for a foil strain gage, with no oxide formations on the surface. A foil strain gage, Micro-Measurements N2A-00-10CBE-350, 3 cm long x 0.3 cm wide, was bonded to the opposite side of the substrate. 24 AWG solid wire was used to connect decade resistor boxes manufactured by Eisco Labs in a Wheatstone bridge setup for the sensor or the foil strain gage. Prior to testing, resistance of the sensor and strain gage was measured and the corresponding decade resistance boxes were set to match. The decade resistor boxes have a resolution of about 1 Ohm. This causes the initial millivolt potential difference to rarely start at zero. To compensate for this, where appropriate, data points were shifted to allow for comparison of different sensors. Constant voltage was provided during testing by B&K precision power supply (1745A). The voltage supply was set to 5 volts for measured resistance above 20 Ohms. For resistance below 20 Ohms, the voltage supply was set to 2 volts. Signals from the drift and strain measurement tests were collected using National Instruments NI cDAQ-9172 board and LabView software. Linearity and sensitivity of the sensor were evaluated using quasi-static loadings. These loadings were carried out using a United SSTM-2K model tensile test machine.

Drift test procedures for the PU/Buckypaper sensor

The mounted sample was connected to the measurement system and placed in a no load and ambient temperature condition for at least 24 hours prior to testing. The test equipment was then turned on, and at least 60 minutes of data were collected for each sample. The drift test was performed several times for the sake of repeatability.

Static test procedures for the PANI/MWCNT sensor

The mounted sample was placed in the tensile testing machine and connected to the measurement system. The system was left idle for at least 1 hour prior to testing in order to remove any accumulated stresses due to mounting. Signal collection was initiated. The tensile test system was set to extend at a rate of 0.001”+/-0.0005” per minute. This way the system was considered to be operating quasistatically. The system was set to increase ramp force at the set extension rate until 350 lbs of force was achieved. The system was then set to instantaneously reduce load to 0 lbs. This procedure was repeated multiple times to determine repeatability of the results and hysteresis in the system.

The drift test was executed for the sample and for the strain gage for a period of 30 minutes or more. The voltage data were captured and for the sensors were shifted so that average recorded signal value was zero. This allowed for direct comparison of the sensors on the graph. The change in voltage per hour for typical results are also tabulated below. The correlation of the data are small because significant noise was generated in the results due to the high sampling rate. Therefore, other measurements given in succeeding sections do not include the correlation values. **Figure 10(a)** shows typical results for one strain gage and two sample sensors. We note that the strain gage showed almost no changes over the test period though there is a slight downward slope to the line. The sample sensors also exhibited very small slopes as well. **Figures 10(b)** and **10(c)** show actual traces for one of the samples and the strain gage where the sensor voltage changes by -0.1298 mV/hr while the foil strain gage changes by -0.0866 mV/hr. The final results of this testing showed that some samples were unstable and had significant drift while others were much more stable but consistently had a drift that was of the same order of magnitude of the strain gage. This is reasonable since our testing apparatus could not be moved and had no way of isolating our samples from outside vibrations. Foil strain gages are known to be stable in this type of environment.

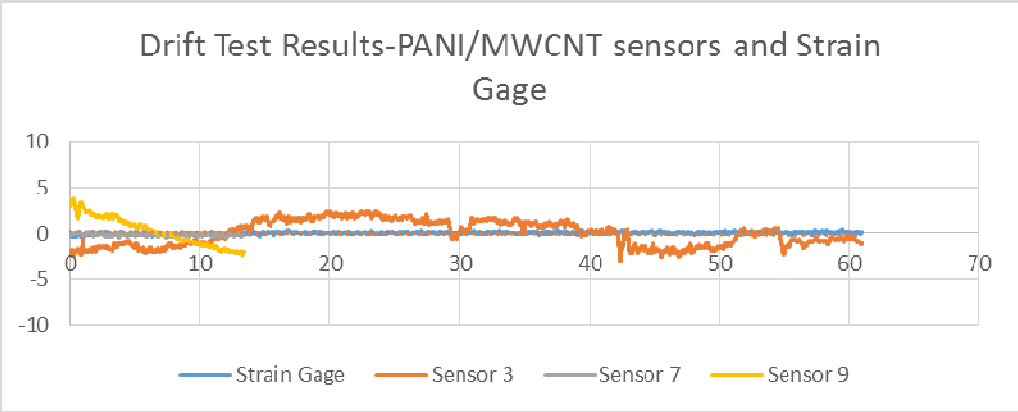

Figure 10(a). PANI/MWCNT sensor and strain gage drift test; a) Drift trendlines for typical PU/Buckypaper sensor and strain gage;

Table 1 Trend line Slopes for Fig. 10(a)

Sample	ΔmV/hour	Sample	ΔmV/hour
Sensor 3 (orange)	-0.1298	Sensor 9 (gold)	-24.008
Sensor 7 (gray)	-0.4353	Strain Gage (blue)	0.1773

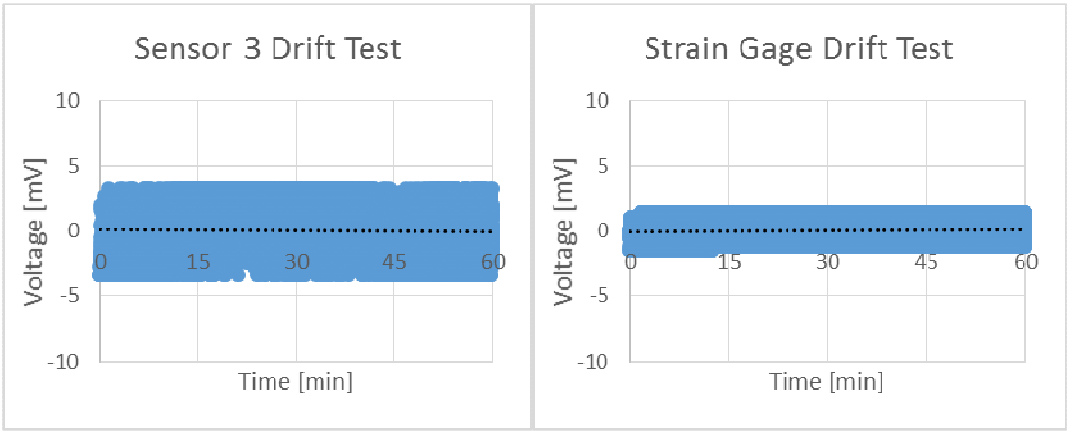

Figure 10 (b) Drift test for PANI/MWCNT sample (sensor 3) and **(c)** Drift test for strain gage.

Load/Unload Testing for the PANI/MWCNT

Linearity and repeatability - static tensile test

Linearity and repeatability are two very important characteristics for strain sensors. It is desirable that the relationship between the applied strain and the output voltage be linear.

The source voltage for the sensor and strain gage in **Fig. 11** are equivalent. **Figure 11** shows typical data for a specific sample that responded as desired. This specific dataset shows six quasi-static loadings and instantaneous unload cycles. **Figure 11** provides typical data obtained from testing both the sample sensor and the strain gauge. Provided are the results of the strain sensing capability of

PANI/11%MWCNT composites sensor and this information is compared to the standard foil strain gage. Each test consisted of a 4-5 minute pre-load preparation period, a three minute loading period and a 3 second unloading period. Generally, both the sensor's and the strain gage's electric resistance change is essentially linear to the applied strain and is related to the gage factor. Whereas the strain gage's gage factor applies over the entire range, for the PANI/11%MWCNT, this must be recalculated over three ranges. The first 4-5 minutes of the test (not shown here) indicate that the system is in pre-load mode and had a residual strain to which both the sensor and strain gage had to adapt before the test is begun. Each unloading occurred about 3 seconds after releasing the previous load. Again, a "no load" pre-load period to set up the next test was introduced before the loading was begun. The strain gage appears to have returned to "zero" but the PANI/MWCNT sensor appears to show some hysteresis. The standard foil strain sensor responded quickly according to the load applied to the beam. However, PANI/MWCNT composites sensor did not completely return to "zero".

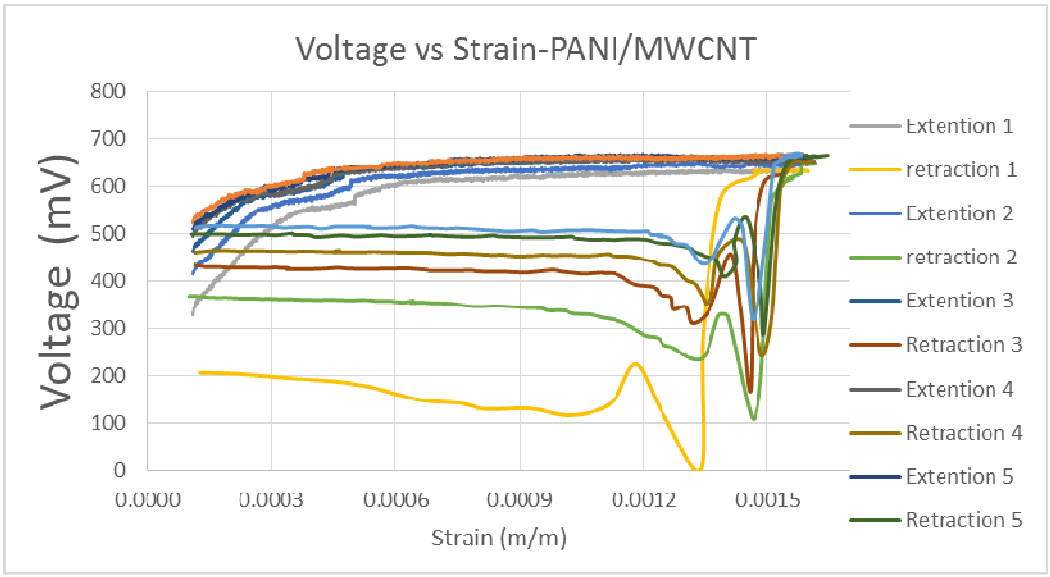

(a)

Table of Slopes and Intercepts for the PANI/MWCNT sensor

Slope [mV/strain]	Run 1	Run 2	Run 3	Run 4	Run 5	Run 6
Section 1	810574	832298	726813	606265	554590	508097
Section 2	270135	212610	216208	184250	210864	190580
Section 3	25577	26860	26117	18852	20537	26283
Intercept [mV]	Run 1	Run 2	Run 3	Run 4	Run 5	Run 6
Section 1	265.91	329.22	393.02	438.98	455.68	476.29
Section 2	440.67	492.51	514.36	528.52	531.09	541.62
Section 3	594.96	607.21	624.92	630.15	635.24	628.53

(b)

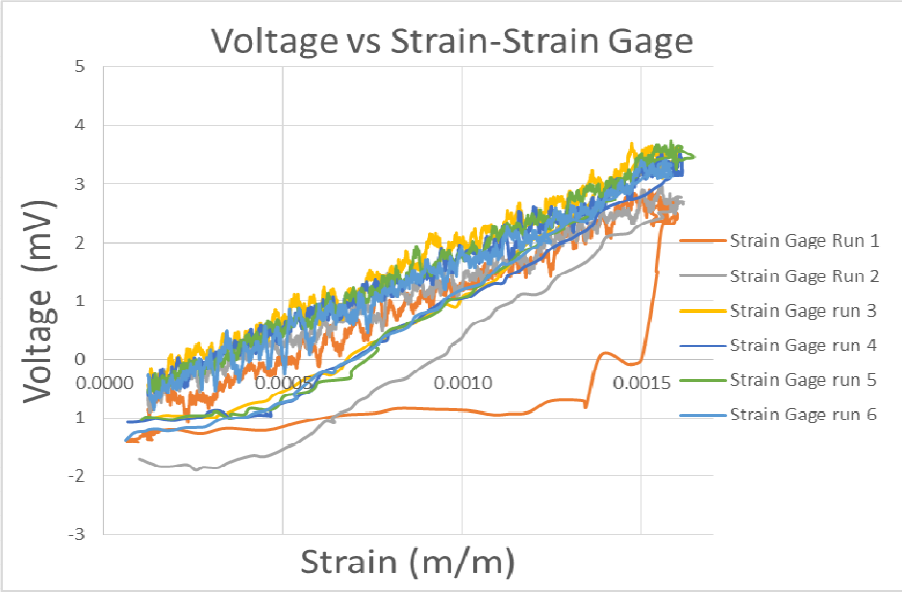

(c)

Figure 11. (a) Voltage-strain curves for the PANI/MWCNT sensor; (b) slopes and intercepts; (c) Voltage-strain curve for strain gage. Note initial linearity of the sensor then marked change in slope in which there is an apparent step, then linear once again at much lower slope. The strain gage shows linear Voltage-strain behavior until unload and returns to the same start value.

As a new load was applied increasing the strain, the PANI/MWCNT composite sensor responded and sensed the strain initially linearly with the input. Yet, the slope for the sensor appears to have 3 distinct regions: rapid change up to strains of 0.0002-0.0004, then a lower slope to about a strain of 0.0004-0.0006, then an even lower slope over the remainder of the test cycle before the load is removed. However, when one evaluates the six cycles we note the similarity of the load-time graphs. We note that the sensor is more sensitive showing changes in voltage that are on several orders larger than those of the strain gage. This is true for all 3 regions. For the strain gage, the results of 6 tests are similar. Therefore, the PANI/MWCNT composite sensor senses similarly to the conventional foil strain gage but the slope of the load displacement curve (i.e., voltage/strain curve) is not uni-valued, though in terms of repeatability and linearity it is repeatable. When one compares the slope of the stress-strain curve in these three regions (not shown here), the slopes are found to be within a few percent of each other.

We also note a small step in the load time curve towards the middle of the second linear region, which indicates that the internal makeup of the PANI/MWCNT undergoes some type of change, perhaps slippage of the MWCNT over each other thereby reducing the sensor gage factor. We also note that when the load is suddenly released a “wave-like” behavior appears in the trace and is due to the tensile machine not having an unloading program that uses an unloading rate that is the negative of the loading rate. Yet, as the sensor cycles through several cycles the unloading trace and the loading trace tend toward stable and similar traces.

Conclusions related the PANI/MWCNT sensor

A PANI/MWCNT sensor was created to evaluate its sensing and damping capabilities versus a standard foil strain gage and constrained layer damping system.

- The free end vibration test results showed that for the single side and double side attachment

damping ratios follow the same trends. However, the double sided attachment has higher values.

- Damping ratios are higher when the sensor is placed at the clamped end.
- The relationship of loss factor, η, and beam coverage L1/L was discussed for single sided and double sided attachment. The loss factor, η, increases with coverage length L1/L increases. The loss factor, η, then decreases before increasing again as the coverage length L1/L continues to increase. The trend for double sided attachment is found to follow the trends discussed by Rao [5] and Levy and Chen [6].
- The PANI/MWCNT sensor's relation between load and displacement or strain is not uni-valued as for a strain gage. It appears to have three regions in which the relationship is quasi-linear. This is in line with an observation given in the previous progress report, namely, adding too much PANI to the sensor patch destroys the linear sensing capability of the sensor patch (item 4 in conclusion section).
- Loading cycle tests showed that though there appears to be residual strain in PANI/MWCNT sensor after the load is removed, the PANI/MWCNT sensor appears to lag behind and shows some hysteresis in the next loading cycle. However, both sensor and the foil strain gage react linearly when re-engaged.
- The dynamic sensing test results showed that over the range of 10-1000 Hz, the PANI/MWCNT composite sensor was consistently superior for sensing purposes since the highest peak consistently corresponded to the input frequency and was much higher than those of the strain gage. In higher frequencies, the composite sensor performed better but the signals were not the largest.
- In the previous progress report we reported that the PANI/MWCNT drift test showed that the sensor was stable over many hours changing by 0.25 mV only over a 20 hour period.
- Lastly, not all samples created were capable sensors. However, the ones that worked produced repeatable results. In comparison to viscoelastic (VEM) constrained layer dampers discussed in [6-7], the same size PANI/MWCNT sensor may not be a weight saver; but is cheaper to produce.

PU/MWCNT Results (submitted for publication)

A second paper based on our research has been submitted to Journal of Nanomaterials titled "Multifunctional Materials of Polyurethane/MWCNT and Evaluation of Damping and Displacement Sensing Properties" [8]. This paper provides the results of our investigations into essentially the same type of topics but evaluates the sensing behavior of the PU/MWCNT sensor, as well.

Polyurethane (PU) has unique dynamic properties in combination with its high load-bearing capacity, properties which were broadly studied for vibration control applications. Studies have been completed testing the damping properties of MWCNT in PU matrix, for example, [9-10]. However, due to the large aspect ratio of the CNTs, the dispersion and directional alignment of the MWCNTs in the polymer matrix is still a great challenge.

Here, a layer by layer attachment method was employed to make PU/Buckypaper composites. A free vibration test method was adopted to study their damping properties. Static and dynamic strain sensing properties were also investigated. One of the advantages of such a composite sensor is its light weight compared to a passively constrained layer damper.

Preparation of PU/Buckypaper

Buckypaper was bought from Nano-lab (Newton, MA, www.nano-lab.com). The procedures to

make Buckypaper is summarized in the paper. The Buckypaper was made of hollow-structured MWCNTs with 15±5 nm outer diameter, about 5-20 microns in length and purity higher than 95%. The thickness of the MWCNT film was around 100 micron and the relative density was about 50%. The Buckypaper was cut into 3.5 cm ×0.9 cm×100 µm sections and placed into 6 cm ×1.3 cm×0.3 cm glass mold very closely.

Four grams PU were dissolved into 50 ml Dimethylformamide (DMF). Four ml of PU/DMF were cast in the Buckypaper filled glass mold. Then, the mold was put in 100 °C oven to dry for 5 h. After that, the PU/MWCNTs were obtained by peeling them off the glass mold. The thickness of the PU is about 80 µm. So, the total thickness of the PU/MWCNTs is around 180 µm. The process is briefly shown in **Fig. 12**.

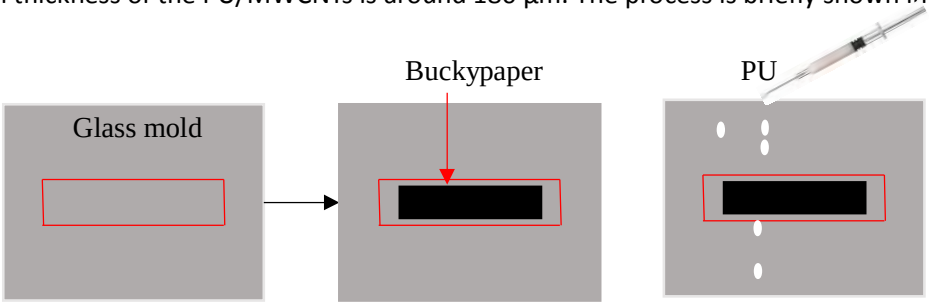

Figure 12. The process of preparation of PU/buckypaper.

Single side attachment mode for PU/Buckypaper

The first single side attachment mode was aimed to compare the differences in performance among pure PU, Buckypaper and PU/Buckypaper composites. Firstly, 3.5 cm × 0.9 cm (length × width) of pure PU, Buckypaper and PU/Buckypaper with 80 µm, 100 µm and 180 µm in thickness, respectively, were attached to 9.5 cm × 0.9 cm × 0.048 cm aluminum base beam single side by a thin layer of adhesive(see **Fig. 13)**. Three very thin layers of nonconductive 3M CA100 liquid instant adhesive were used to cover these samples to separate the samples from the environment. Each specimen was dried in room temperature for 24 hrs. The base beam material used was made of 6061-T6 Aluminum. The red dashed lines shown in **Fig. 14** defined the locations where the beam was clamped. The side of the Aluminum base beam without the attachment of samples were tested then cut 1 cm at a time and the results were compared. The unclamped side was then made to vibrate and the damping ratio was determined.

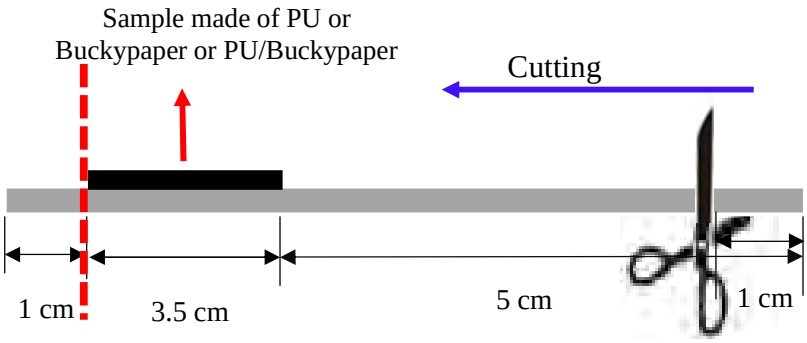

Figure 13. Schematic images of single side attachment. The dimension of samples, Al beams and the locations where samples were attached, the locations (red line) where the beam was clamped and also the directions and lengths for beam removal.

The second single side attachment mode was built to investigate how the damping changed as a function of the coverage of PU/Buckypaper to aluminum base beams. The PU/Buckypaper with dimension of 3.5 cm × 0.9 cm × 0.018 cm was attached upon a 20.5 cm × 0.9 cm × 0.048 cm Aluminum base beam on one side (see **Fig. 14**) using a thin layer of glue as discussed in the previous paragraph. The specimen was dried at room temperature for 24 hrs. Free vibration comparisons were made by using either the sample side, #, or the uncovered side, *, alternately, as the fixed support for the cantilever beam. The red dashed lines shown in **Fig. 14** defined the locations where the beam was clamped. The side of the Al base beam without the attachment of samples were either cut or clamped 1 cm at a time until the clamp was next to the sample. The unclamped side was then made to vibrate and the damping ratio was determined and the results were compared.

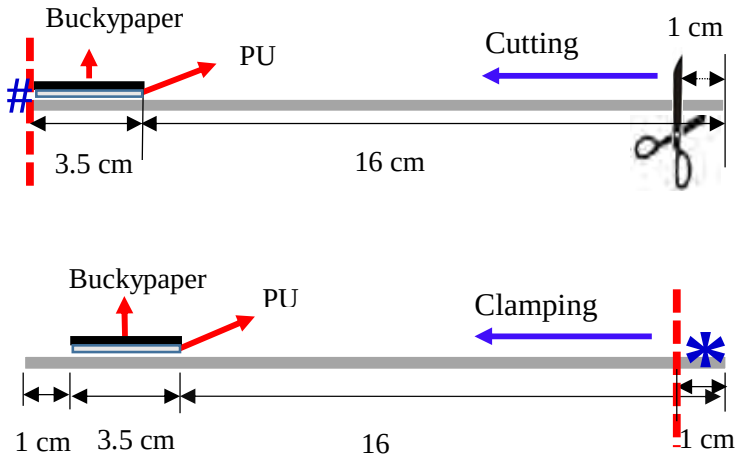

Figure 14. Schematic images of single side's attachment. The dimension of samples, Al beams and the locations where samples were attached, the locations of sample side, #, and free end side, *, where the beam was clamped and also the directions and lengths for both beam removal and clamping.

Double sided attachment mode for PU/Buckypaper

All the dimensions of sample and aluminum base beams, the clamped locations and the directions and lengths for both cutting and clamping are kept the same as the second single side attachment mode described above. The only change that was made was that the aluminum base was covered on both sides by the sample (See **Fig. 15).**

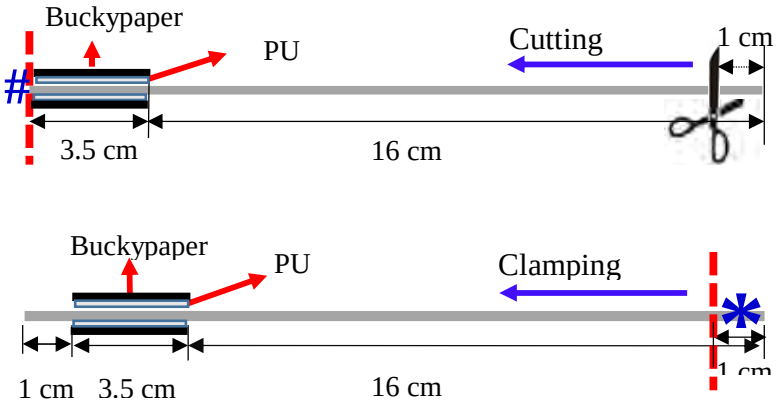

Figure 15. Schematic images of double sides' attachment. The dimension of samples, Al beams and the locations where samples were attached, the locations of sample side, #, and free end side, *, where the beam was clamped and also the directions and lengths for both beam removal and clamping.

Damping Test Methodology

The cantilever beams of **Figs. 13, 14 and 15** were given the same small initial displacement and then released for free vibration. Unclamped end displacements were measured by a laser vibrometer and a two channels digital oscilloscope was used to display and store the signal. Five trials were made for each setup and the mean value of the damping ratio was calculated. This ratio can be related to the logarithmic decrement of consecutive maxima of end displacements and can be correlated to how much vibration energy is removed from the sample. The higher the damping ratio, the better the sample acts as a damper.

Damping ratios of PU, Buckypaper and PU/Buckypaper composites

The free end vibration test has already shown that the Buckypaper has strain sensing properties [11]. Also, PU has excellent damping ability which is broadly studied. Herein, the free end vibration test method was adopted to study the damping behaviors of PU, Buckypaper and their layer by layer PU/Buckypaper composite. For the Al base beam the single side attachment test free vibration trial results are shown in **Fig. 16** (see **Fig. 13** for the configuration of the tests setup)**.**

Five trials were run for each of clamping boundary conditions previously defined and damping ratio was obtained. Standard deviation is also shown in **Fig. 16.** The Buckypaper has slightly higher damping ratios than PU. However, it is clearly shown that PU/Buckypaper composite has significantly higher damping ratios than both of their pure components (PU and Buckypaper). The damping ratios increased as the sample coverage decreased in the range of 63.6% to 41.2% with its pure components. We can see that the Buckypaper acts as a constraining layer and the PU acts similar to a viscoelastic layer.

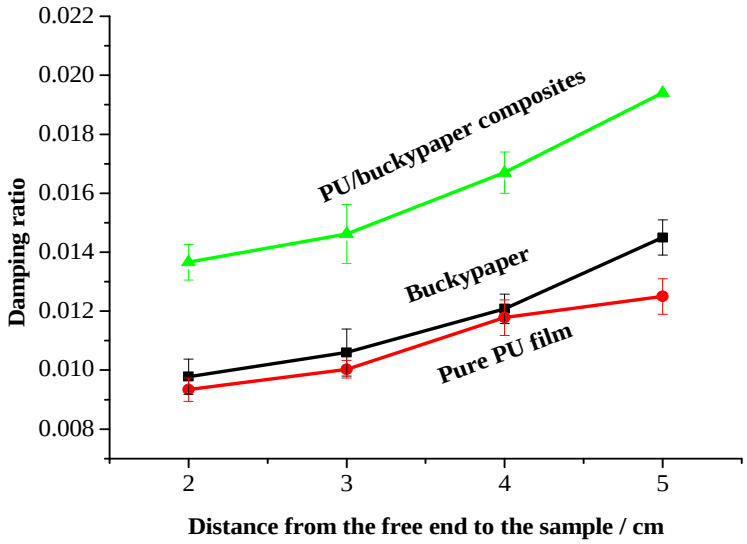

Figure 16. Damping ratios comparison of PU, Buckypaper and PU/Buckypaper composites.

Damping results for single side attachment for the PU/Buckypaper

As mentioned previously, the reason for the creation of the composite is for use as a sensor-actuator with damping capabilities. To check on the damping capability aspect, several tests were performed. For the Aluminum base beam single sided attachment test (see **Fig. 14** for the configuration of the tests setup), free vibration trial results are shown in **Fig. 17.**

Five trials were run for each of the clamping conditions listed. The results clearly showed that the damping ratio initially increased as the distance from the free end to the sample decreased for both clamping on the free end side, *, and clamping on the sample side, # (see **Fig. 17**). Then, it decreased as the distance from the free end to the sample further decreased for both clamping on the free end side, *, and clamping on the sample side, #. For both clamping on the free end side, * and clamping on the sample side, #, the damping ratio reached the highest values 0.0124 and 0.0202, respectively, when the distance from the free end to the sample is 6 cm. Comparing the highest damping ratios, 0.0124 and 0.0202, when the distance from the free end to the sample is the same 6 cm, it is determined that clamping on the sample side, #, has 162.9% higher damping ratio than when clamping on the free end side, *. The trends follow previous published results for constrained layer viscoelastic dampers.

There is a further increase of the damping ratio after it decreases for the case where the clamping is on the free end side, *. This is reasonable when compared with the trend of the damping ratio of clamping on the sample side. The damping ratios remain lower for each new beam length trial when clamped on the free end side compared with the value for each beam length trial when clamped on the sample side. However, the damping ratios have to be the same when the beam being tested becomes symmetric with respect to the vertical axis; meaning, it doesn't matter whether you test the clamped side or the free end side, both will be the same configuration leading to the same damping ratio.

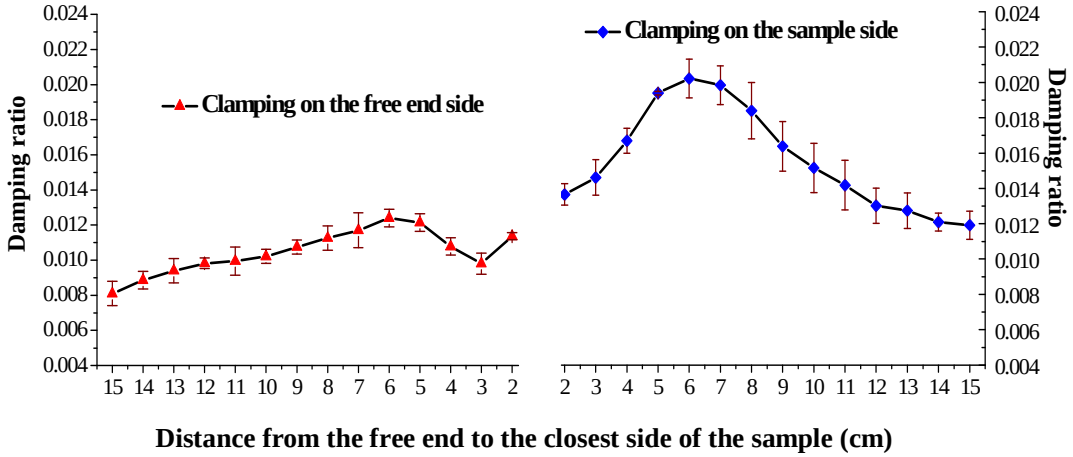

Figure 17. Damping ratios of single side attached PU/Buckypaper clamped on the free end side, *, and the sample side, #.

Damping results for single side attachment for the PU/Buckypaper

The double sides' attachment experimental setup is shown in **Fig. 15.** The damping ratio results given in **Fig. 18** display the same trend as the damping ratios for single sided attachment. However, the double sides' attachment has higher damping ratios compared with single side attachment. It reaches the highest damping ratio of 0.033 with double sides' attachment when the sample's right end is 3 cm

away from the free end. Also, the damping ratio differences between clamping on the sample side and clamping on the free end for the same distance from the free end to the sample is bigger for double sided attachment than the single sided attachment. An increase in damping ratio when clamped on the free end side is noted, which is just like the single side attachment trend. The Y-coordinate value is very close at the 0 cm value of X-coordinate, which is expected.

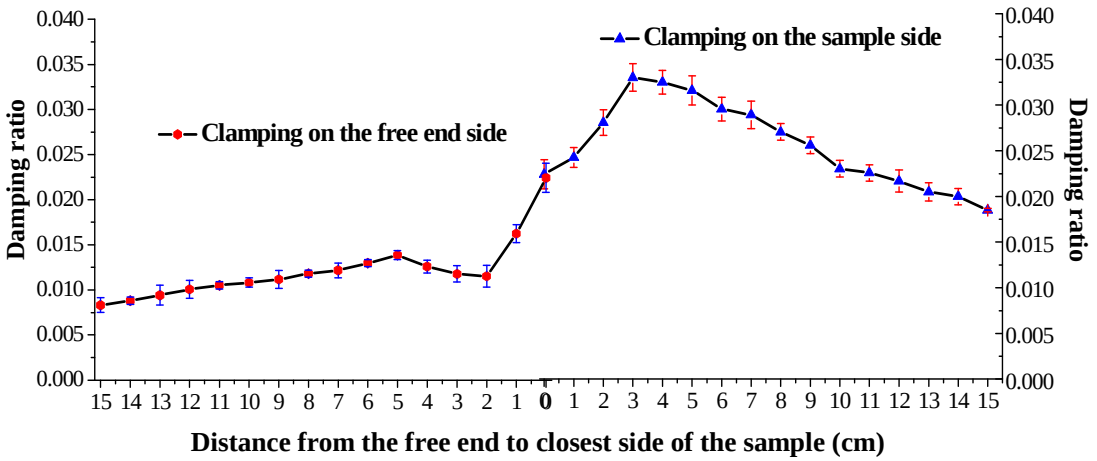

Figure 18. Damping ratios of double sides attached PU/Buckypaper clamped on the uncovered side, *, and sample side, #.

When one compares the loss factor as a function of the non-dimensional coverage length in both these cases, the graphs of **Fig. 19** are obtained. Here, the loss factor, η, is twice the damping ratio for small damping ratios up to 0.3 [5]. We note the similarity in trends of the loss factor for the sample side clamping condition, #, when compared to Chen and Levy [7]. First the double sided coverage produces a higher loss factor which increases as the sample length to the beam length (L1/L) increases and then begins to decrease as L1/L tends to 1.

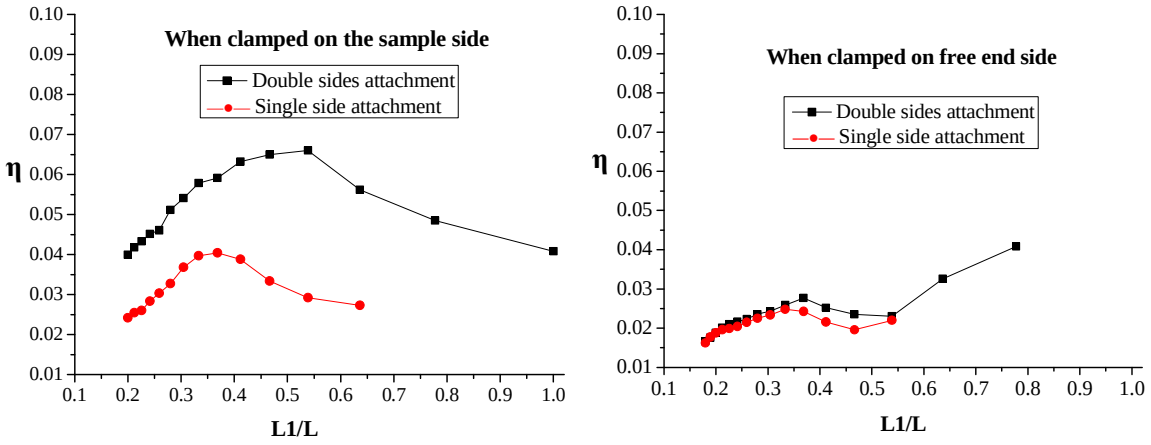

Figure 19. Comparison between single side and double sided attachment of the PU/Buckypaper sample for both clamping conditions

An analysis of the loss factor versus non-dimensional coverage length when clamping is on the free

end side, *, is now undertaken. This analysis applies for the single side and also for the double side coverage, as well. The loss factor for small L1/L can best be described as that for a sample starting to act as a passive layer type damping element and as an end mass. But as the beam material is removed, thereby increasing L1/L, the loss factor of the sample transitions to more of a loss factor for a passive layer type damping element covering more and more of the beam. We note that the loss factor, η, first increases with coverage length, L1/L, though its value is several times smaller than its value when the beam is clamped on the sample side. In this configuration the sample acts as a small mass at the end of the beam and coverage length effects dominate. Then the loss factor decreases to a minimum value before increasing again as L1/L, the dimensionless coverage length, increases. This decrease may be due to the fact that as more beam is removed, the sample starts to act as a larger end mass compared to the mass of the beam and that becomes the dominating effect. Such a system will tend to execute relatively larger end displacements, and, according to Rao [5], for viscoelastic materials, this implies a lower loss factor (see [5], pg. 686). As more beam material is removed, a second increase occurs in the loss factor due to the sample transitioning from being like an end mass to beginning to cover the majority of the beam. This behavior is similar to that found in Chen and Levy [6] for the vibration of a viscoelastic constrained layer damping of a beam with end mass. However, this increase-decrease-increase phenomenon in the loss factor is noticed for both the single side and double side coverage of the beam. Though [6,7] investigated the change in L1/L by increasing L1 and keeping L fixed, the behavior seen in this investigation can be deduced from the results found in [6,7] and follow the trends therein. However, the differences in loss factor between single sided and double sided coverage were much larger in [7] compared to what is noted here because of the materials used. Yet, the trends in [7] and shown in this work are very similar.

Static sensing properties -The drift effect

The stability of each sensor was tested and typical results for some samples and strain gage are discussed following explanations of the test procedures.

Sample Setup for drift, static tensile test, and dynamic tests for the PU/Buckypaper

The sensor was bonded to the center of a 61 mil thick 6061-T6 Aluminum rectangular bar using 3M CA100 liquid instant adhesive. Each specimen was held in place by a weight and dried in room temperature for 24 hrs. The bonding area was prepared to ensure a smooth surface, as is normally defined for a foil strain gage, with no oxide formations on the surface. A foil strain gage, Omega SGD-30/350-LY40, 3 cm long x 0.3 cm wide, was bonded to the opposite side of the substrate. 24 AWG solid wire was used to connect decade resistor boxes manufactured by Eisco Labs in a Wheatstone bridge setup for the sensor or the foil strain gage. Another strain gage supplier was used due to problems obtaining strain gages used for previous tests. Prior to testing, resistance of the sensor and strain gage was measured and the corresponding decade resistance boxes were set to match. The decade resistor boxes have a resolution of about 1 Ohm. This caused the initial millivolt potential difference to rarely start at zero. To compensate for this, where appropriate, data points were shifted for comparison of different sensors. Constant voltage was provided during testing by B&K precision power supply (1745A). The voltage supply was set to 5 volts for measured resistance above 20 Ohms. For resistance below 20 Ohms, the voltage supply was set to 2 volts. Signals from the drift and strain measurement tests were collected using National Instruments NI cDAQ-9172 board and LabView software. Signals from the Dynamic sensing tests were collected using Data Translation DT9837C and SpectraPLUS-DT. Linearity and sensitivity of the sensor were evaluated using quasi-static loadings. These loadings were carried out using a United SSTM-2K model tensile test machine.

Drift test procedures for the PU/Buckypaper sensor

The mounted sample was connected to the measurement system and placed in a no load and ambient temperature condition for at least 24 hours prior to testing. The test equipment was then turned on, and at least 30 minutes of data were collected for each sample. The drift test was performed several times for the sake of repeatability.

Static test procedures for the PU/Buckypaper sensor

The mounted sample was placed in the tensile testing machine and connected to the measurement system. The system was left idle for at least 1 hour prior to testing in order to remove any accumulated stresses due to mounting. Signal collection was initiated. The tensile test system was set to extend at a rate of 0.001"+/-0.0005" per minute. This way the system was considered to be operating quasistatically. The system was set to increase ramp force at the set extension rate until 350 lbs of force was achieved. The system was then set to instantaneously reduce load to 0 lbs. This procedure was repeated multiple times to determine repeatability of the results and hysteresis in the system.

The drift test was executed for the sample and for the strain gage for a period of 30 minutes or more. The voltage data were captured and for the sensors were shifted so that average recorded signal value was zero. This allowed for direct comparison of the sensors on the graph. The change in voltage per hour for typical results are also tabulated below. The correlation of the data are small because significant noise was generated in the results due to the high sampling rate. Therefore, other measurements given in succeeding sections do not include the correlation values. **Figure 20(a)** shows typical results for one strain gage and two sample sensors. We note that the strain gage showed almost no changes over the test period though there is a slight downward slope to the line. The sample sensors also exhibited very small slopes as well. **Figures 20(b) and 20(c)** show actual traces for one of the samples and the strain gage where the sensor voltage changes by -0.6184 mV/hr while the foil strain gage changes by -0.0866 mV/hr. The final results of this testing showed that some samples were unstable and had significant drift (not shown on graph) while others were much more stable but consistently had a drift that was one order of magnitude larger than that of the strain gage. This is reasonable since our testing apparatus could not be moved and had no way of isolating our samples from outside vibrations. Foil strain gages are known to be stable in this type of environment.

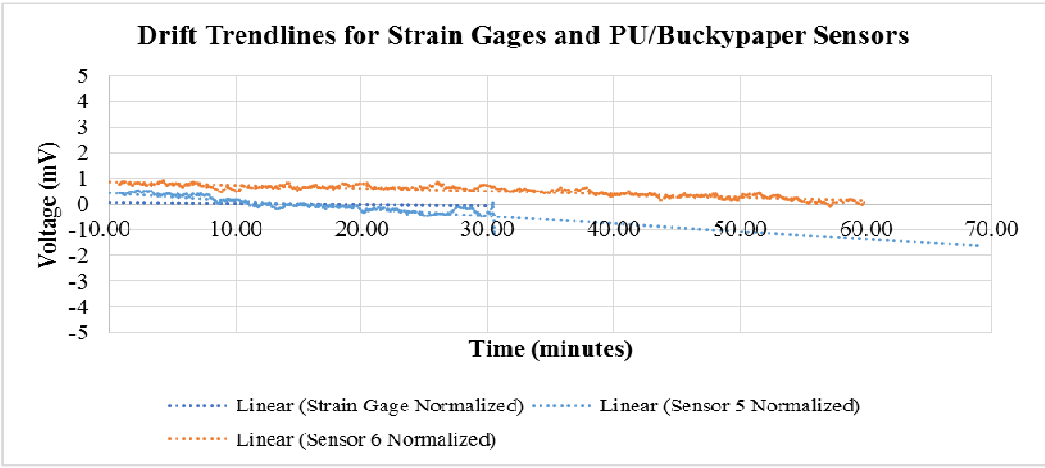

Figure 20(a). PU/Buckypaper sensor and strain gage drift test; a) Drift trendlines for typical PU/Buckypaper sensor and strain gage;

Table 2 Trend line Slopes for Fig. 19(a)

Type of Sample	Δ mV/hour	Type of Sample	Δ mV/hour
PU/Buckypaper-blue line	-0.6184	**PU/Buckypaper-black line**	-1.7925
Strain Gage-green line	0.0866		

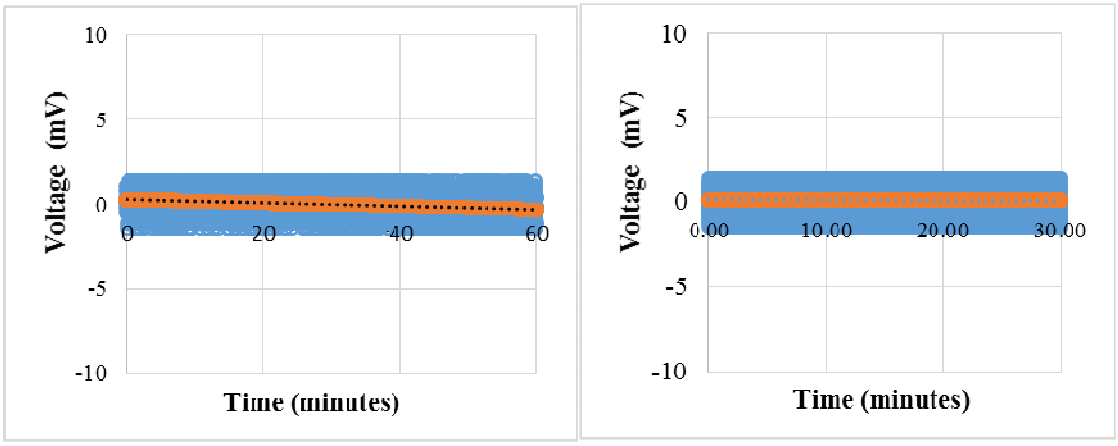

Figure 20 (b) Drift test for PU/Buckypaper sample (sensor 5) and 20**(c)** Drift test for strain gage.

Linearity and repeatability - static tensile test

Linearity and repeatability are two very important characteristics for strain sensors. It is desirable that the relationship between the applied strain and the output voltage be linear.

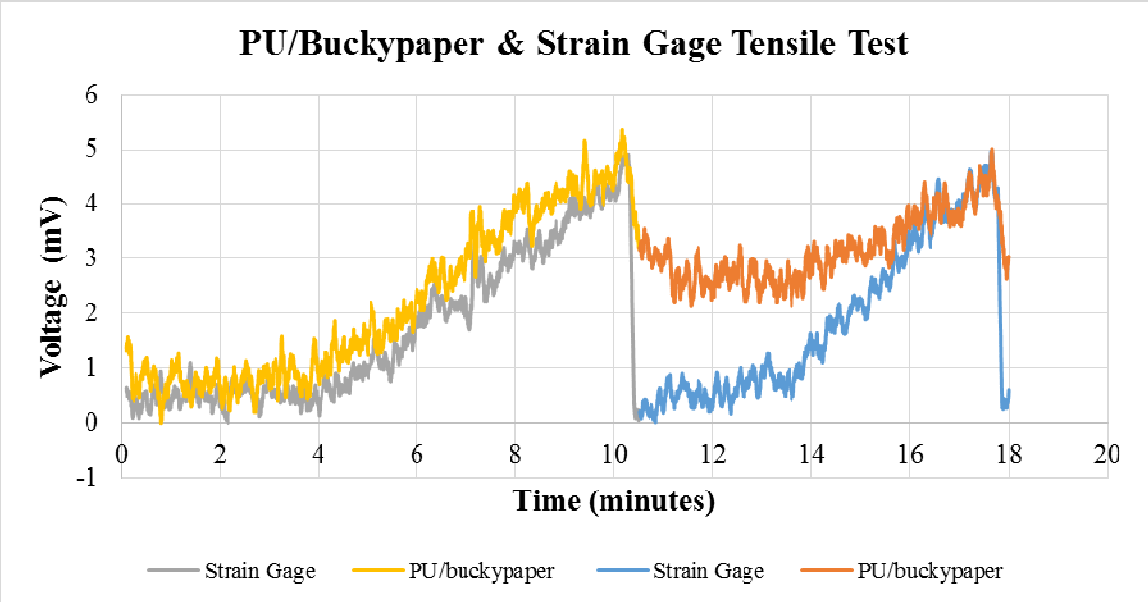

Figure 21(a). The repeat loading comparison of PU/Buckypaper and standard foil strain gage-the raw data

The source voltage for the sensor and strain gage in **Fig. 21** are equivalent. **Figure 21** shows typical data for a specific sample that responded as desired. This specific dataset shows two quasi-static

loadings and instantaneous unload cycles. **Figure 21** provides typical data obtained from testing both the sample sensor and the strain gauge. Provided are the first loading tensile test in which the strain sensing behavior of PU/Buckypaper composites sensor is similar to the behavior of the conventional foil strain gage. Generally, both the sensor's and the strain gage's electric resistance change is essentially linear to the applied strain and is related to the gage factor. The first 4 minutes of the test indicate that the system had a residual strain that required both the sensor and strain gage to adapt to before the test was begun. The second loading occurred about 3 seconds after releasing the previous load. Again, a "no load" time period between the 10th and the 13th minute was introduced before the loading was begun again. The strain gage appears to have returned to "zero" but the PU/Buckypaper sensor appears to lag behind and shows some hysteresis. The conventional foil strain sensor responded quickly according to the load applied to the beam. However, PU/Buckypaper composites sensor did not completely return to "zero". As a new load was applied increasing the strain, the PU/Buckypaper composite sensor responded and sensed the strain linear with the input. Yet, the slope for the sensor appears to be different than during the first load cycle. Hence, both sensors have a linear voltage output. By factoring out the lag in response of the second loading, all four output trend lines are deemed relatively parallel (**Fig. 21(b)**). Since the input voltage and output voltage is equivalent or relatively similar, so are the gage factors. Therefore, the PU/Buckypaper composite sensor senses similarly to the conventional foil strain gauge in terms of repeatability and linearity.

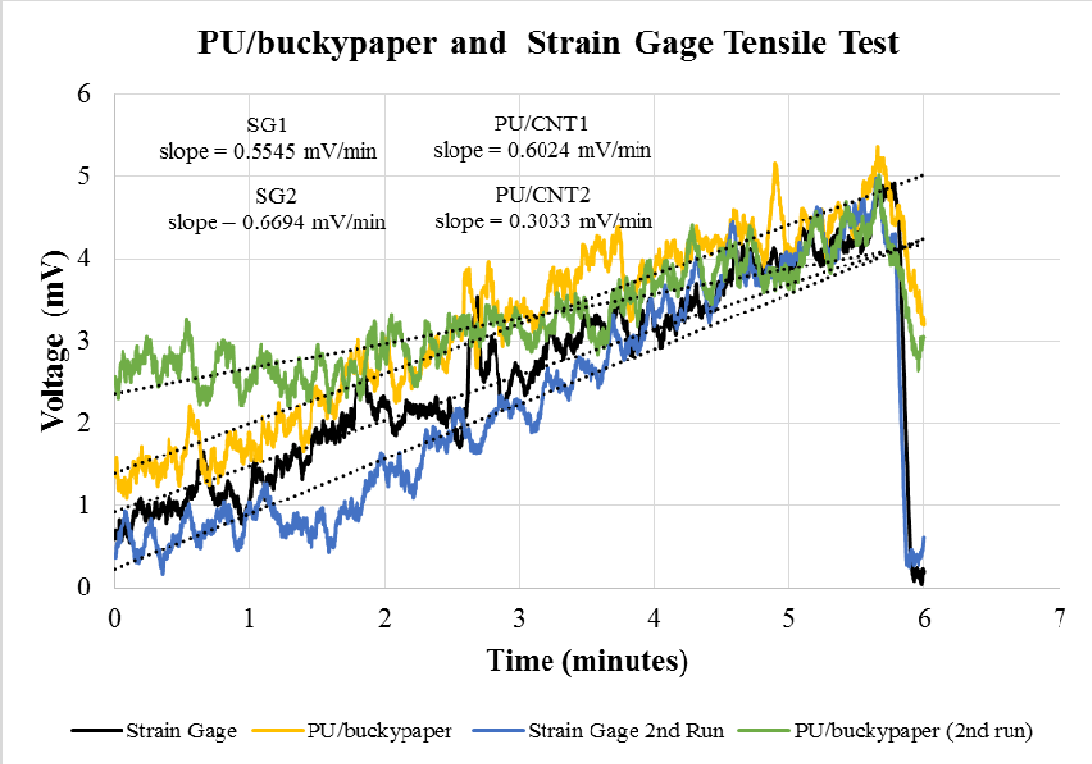

Figure 21(b). The repeat loading comparison of PU/Buckypaper and standard foil strain gage-data linearity

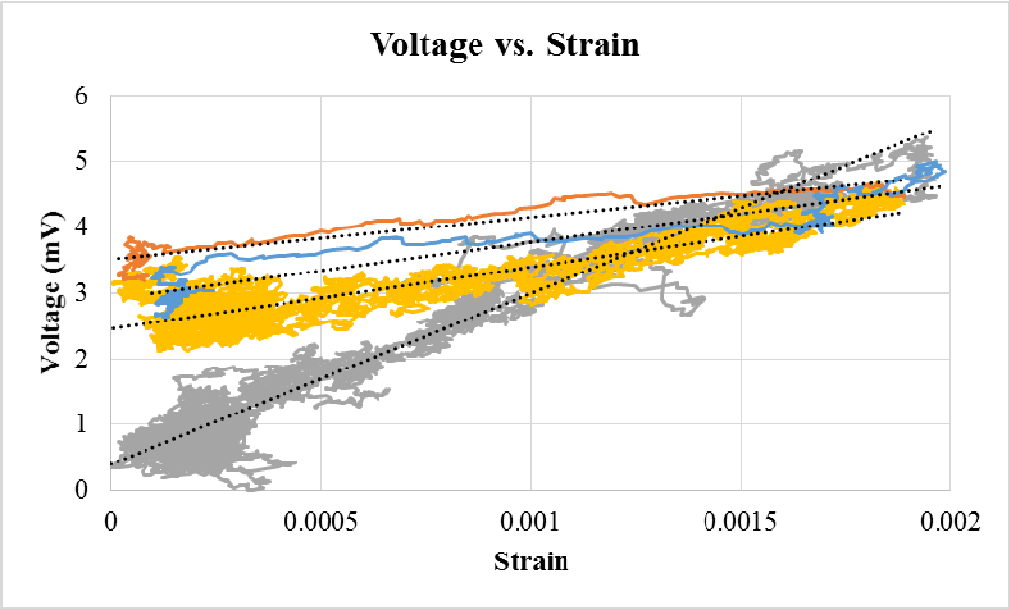

Slope mV/ (m/m)	Load1	2600	Unload1	640	Load2	932	Unload2	857

Figure 21(c). The loading/unloading comparison of PU/Buckypaper versus strain--first load (gray)/unload (red) and second load (yellow)/unload (blue) of the sensor.

Dynamic sensing characteristic--Dynamic test procedures for PU/Buckypaper

The sample was mounted onto a cantilever beam system. The sensor was located as close as possible to the fixed end. The free end was attached to a vibration drum that vibrates at specified frequencies. An accelerometer was attached to the free end, as close to the center of the vibration drum as possible. The accelerometer linked into a feedback loop that ensured that the acceleration of the free end was correct as per the frequency versus acceleration profile. This profile was set up such that the acceleration started at 10 Hz and 10 g's, ramped up to 20 Hz and 20 g's, then held a constant acceleration of 20 g's from 20 Hz to 6000 Hz. The control system was then set to run a specified frequency. The resulting signals were collected and analyzed using the Hanning FFT algorithm. The peak hold data for the signals were collected over the course of 500 signal samples using a sampling rate of 11000 Hz for an input frequency range of 10 to 1000 Hz and 60000 Hz for an input frequency range of 1000 to 5000 Hz. Five sets of peak hold data were taken and analyzed.

Results found

Dynamic response performance is the importance criterion for sensors. Standard foil strain gages are used for comparison. The frequency to be evaluated was input into the system and held for a period of time until stable. That frequency was then used to study the sensitivity of the PU/Buckypaper and the foil strain gages to input frequencies. Frequency domain from 10 Hz to 1000 Hz was investigated and the results are presented in **Fig. 22**. The FFT graphs consistently showed a response at 60 Hz of 0.418 mV for the PU/Buckypaper composite sensor and 1.47 mV for the foil strain gage. This response is due to background source that is always present and can be disregarded.

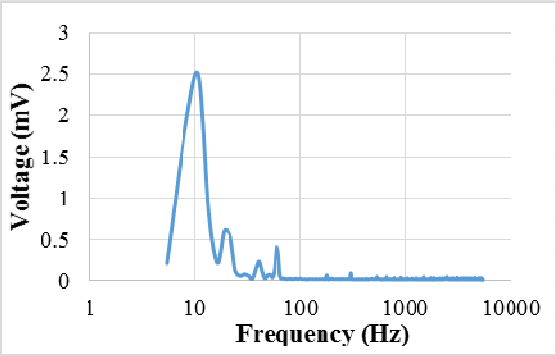

a) 10 Hz – PU/Buckypaper – Magnitude: 2.4727 mV

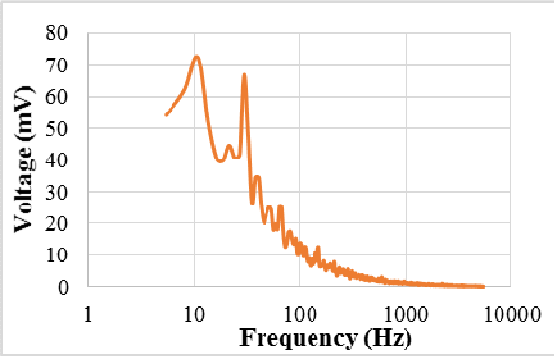

b) 10 Hz – Foil Strain Gage – Magnitude: 70 mV

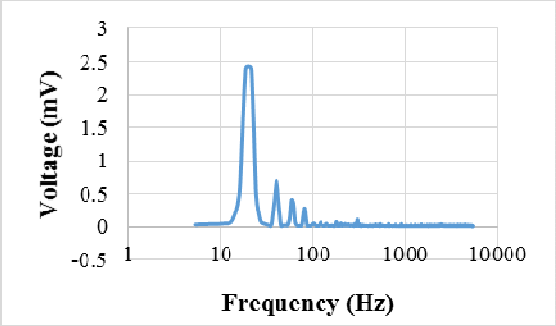

c) 20 Hz – PU/Buckypaper – Magnitude: 2.4082 mV

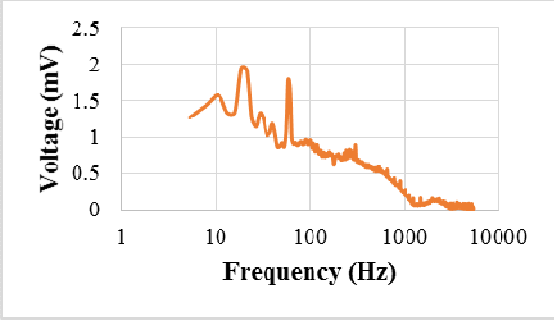

d) 20 Hz – Foil Strain Gage – Magnitude: 1.9579 mV

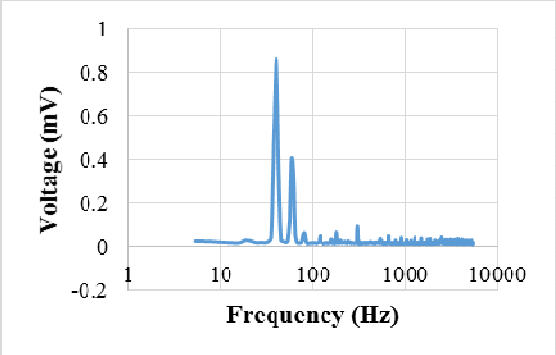

e) 40 Hz – PU/Buckypaper – Magnitude: 0.8601 mV

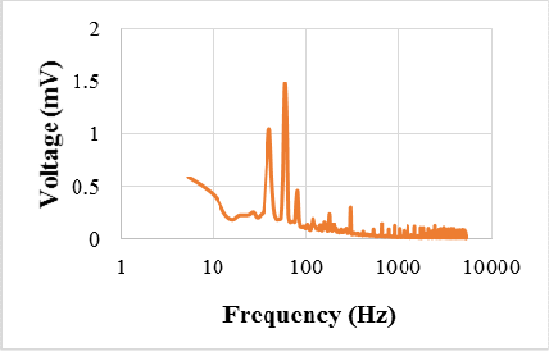

f) 40 Hz – Foil Strain Gage – Magnitude: 1.0515 mV

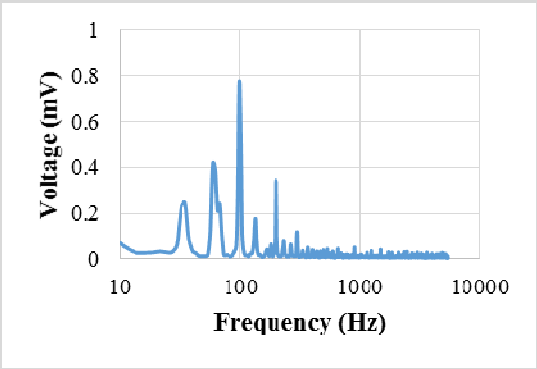

g) 100 Hz – PU/Buckypaper – Magnitude: 0.7716 mV

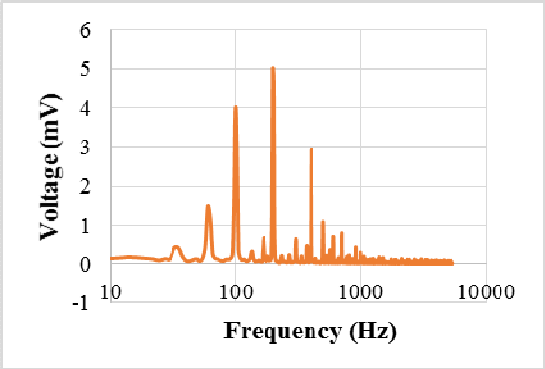

h) 100 Hz – Foil Strain Gage – Magnitude: 3.9748 mV

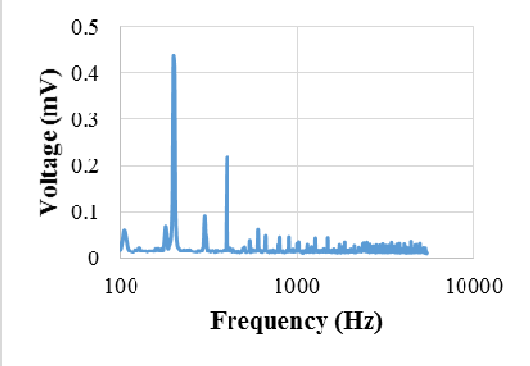

i) 200 Hz – PU/Buckypaper – Magnitude: 0.4374 mV

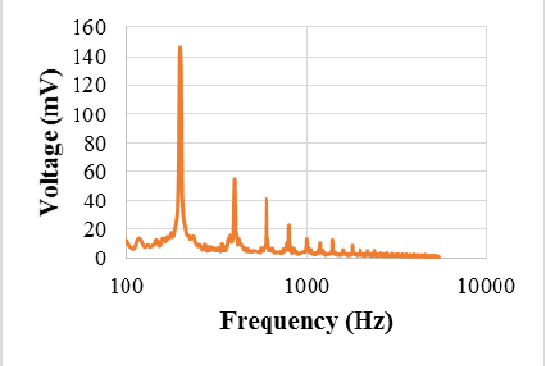

j) 200 Hz – Foil Strain Gage – Magnitude: 145.43 mV

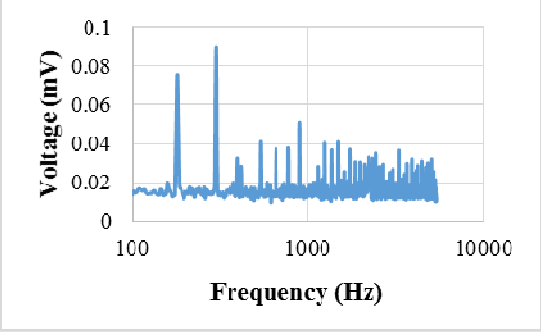

k) 400 Hz – PU/Buckypaper – Magnitude: 0.0325 mV

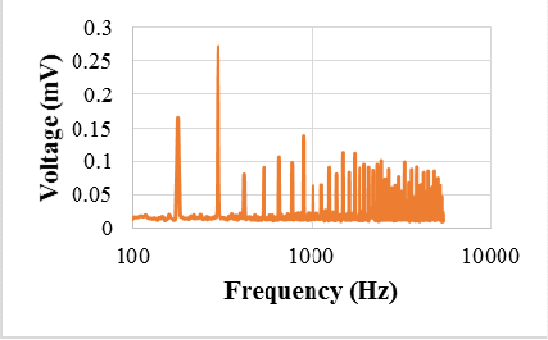

l) 400 Hz – Foil Strain Gage – Magnitude: 0.0229 mV

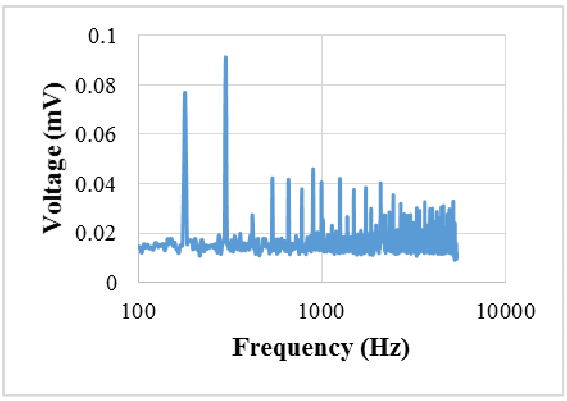

m) 1000 Hz – PU/Buckypaper – Magnitude: 0.0403 mV

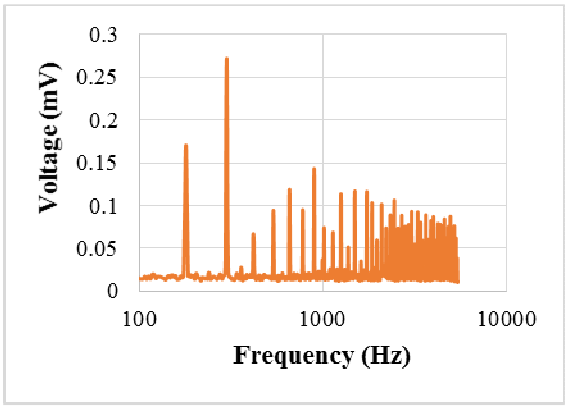

n) 1000 Hz – Foil Strain Gage – Magnitude: 0.0365 mV

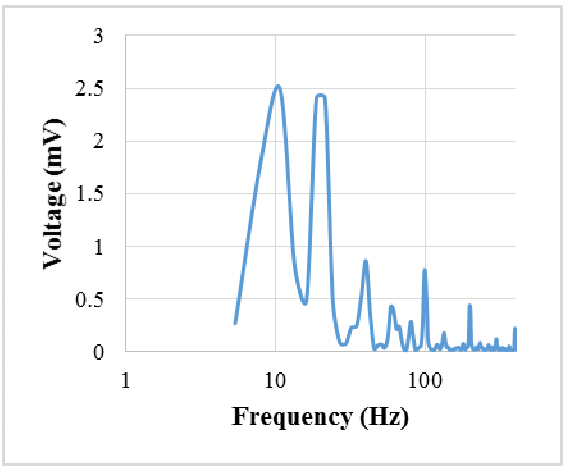

o) FRF superposition-PU/Buckypaper sensor (10-400 Hz)

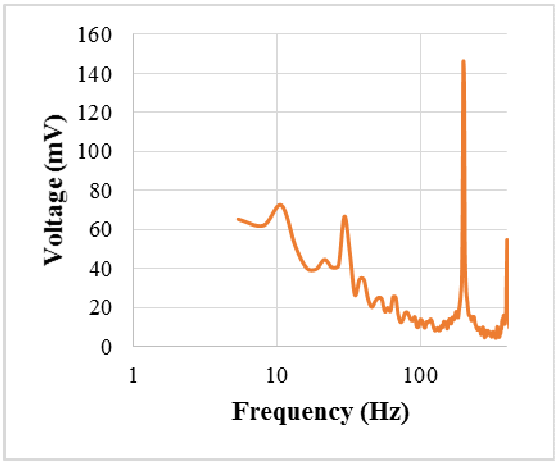

p) FRF superposition – Foil strain gage (10-400 Hz)

Figure 22. Comparison the frequency response of the standard foil strain gages and of the PU/Buckypaper composites.

The results displayed in **Figs. 22(a)-(n)** are typical results for the sensor and strain gage. Over the range of 10 Hz to 200 Hz, the PU/Buckypaper composite sensor is either the same or is superior for sensing purposes since the highest peak consistently corresponds to the input frequency. The foil strain gage is superior at 10 Hz and 200 Hz in the sense that it gives a significantly larger voltage response when compared to the composite sensor. In higher frequencies, the composite sensor either performed similarly well or both signals were not detectable to any accuracy for sensing.

When the frequency is increased, the voltage output for both strain gage and PU/Buckypaper composites decreases greatly. The voltage output of PU/Buckypaper composites dropped to 0.77 mV with frequency of 100 Hz and the strain gage drops to about 3.98 mV. When the frequency is further increased to 1000 Hz, the voltage output of both sensors remain of the same order, 0.0403 vs. 0.0365 mV. It means that the PU/Buckypaper composites strain sensors may be better for structural health monitoring, which frequently uses the change of the natural frequency as an index for detecting small cracks (e.g., [12-14]).

The FRFs shown in **Figs. 22 (a)-(n)** are superposed and given in **Figs. 22(o)** and **22(p)** and represent the response of PU/Buckypaper or of the strain gage, respectively, to the different input frequencies. This is not a true FRF because the frequency sweep method must be used to generate these graphs. The graphs show a fuller picture of the dynamic sensing capabilities of each sensor. This is advantageous for the comparison of the sensor and strain gage because it shows how the signal could be used for frequency sensing. The graph for the PU/Buckypaper composite sensor shows a sensor that responds to frequencies in the range of 10 to 200 Hz while at the same time having each frequency signal distinguishable from each other. The foil strain gage does not have this capability. The 10 Hz foil strain gage response eclipses all the frequency responses up to 200 Hz and appears to show a peak at 30 Hz, a frequency for which no sampling was made. For the reasons stated, the PU/Buckypaper composite sensor responds in a superior manner when compared to a foil strain gage.

Conclusions related to PU/Buckypaper

A PU/Buckypaper sensor was created to evaluate its sensing and damping capabilities versus a standard foil strain gage and constrained layer damping system.

- The free end vibration test results showed that for the single side attachment, the damping ratios for both PU film and Buckypaper are close, while PU/Buckypaper composites have higher damping ratios than their individual components.
- For both single side attachment and double sided attachment, the damping ratios when clamping on the sample side are much higher than when clamping on the free end side.
- The relationship of loss factor, η, and beam coverage L1/L was discussed for single sided and double sided attachment. The loss factor, η, increases with coverage length L1/L increases. The loss factor, η, then decreases before increasing again as the coverage length L1/L continues to increase. The trend for double sided attachment is found to follow the trends discussed by Rao [5] and Levy and Chen [6].
- The possibility of PU/Buckypaper to be used as a strain sensor was also investigated. Though, there is a drift for the PU/Buckypaper sensor during the one hour long drift test, the slope is relatively small.
- Two loading cycle tests showed that though there are residual strain for both PU/Buckypaper sensor and standard foil strain sensor for both loading cycles, the PU/Buckypaper sensor appears to lag behind and shows some hysteresis in the second loading cycle. However, both sensors had a linear voltage output and all four output trend lines are deemed relatively linear and in the first cycle also parallel. Therefore, the PU/Buckypaper composite sensor senses similarly to the standard foil strain gauge in terms of repeatability and linearity.
- The dynamic sensing test results showed that over the range of 10 Hz to 200 Hz, the PU/Buckypaper composite sensor was comparable to or superior for sensing purposes since the highest peak consistently corresponded to the input frequency. In higher frequencies, the composite sensor either performed better or both signals were not detectable to any accuracy for sensing. It means that the PU/Buckypaper sensor has the potential to be strain sensor.
- Lastly, not all samples created were capable sensors. However, the ones that worked produced repeatable results. In comparison to viscoelastic (VEM) constrained layer dampers discussed in [6, 7], the same size PU/Buckypaper sensor would have a density that is 40% of the VEM and 6.4% of the density of the constraining layer, would have similar damping behavior, but would have more useful attributes for a sensor.

Investigation of other combinations including DYAD VEM (to be published)

Single side's attachment mode of Buckypaper/DYAD/ (PANI/MWCNT) and Buckypaper/DYAD/Buckypaper nanocomposites films

A new composite system was also investigated using some of the components we have been working with and the addition of the DYAD viscoelastic material used by Chen and Levy [6, 7]. Layer-by-layer attachment method was adopt to make Buckypaper/ DYAD/ (PANI/MWCNT) and Buckypaper/ DYAD/ Buckypaper nanocomposites films. The creation of the PANI/MWCNT was the same as described previously using frit compression force of 75 lbs in this case. Simply, 3 cm × 0.9 cm × 100 µm of Buckypaper was bonded to one side of 6061-T6 Aluminum beam (dimension: 1.25 mm ×0.9 cm in thickness × varying length) using 3M CA100 liquid instant adhesive. DYAD bought from Soundcoat, Inc., was cut to the same dimension as the Buckypaper and was glued with one layer of the liquid adhesive onto the attached Buckypaper. After that, the prepared PANI/MWCNT or another layer of Buckypaper was bonded upon the DYAD. Three very thin layers of nonconductive 3M CA100 liquid instant adhesive were used to cover these samples to separate the samples from the environment. After drying for 24 h at room temperature, the single side attached of Buckypaper/DYAD/ (PANI/MWCNT) nanocomposites and Buckypaper/DYAD/Buckypaper nanocomposites films were built (see **Fig. 23** below). Free vibration comparisons were made by using either the sample side, #, or the uncovered side, *, alternately, as the fixed support for the cantilever beam. The red dashed lines shown in **Fig. 23** defined the locations where the beam was clamped. The side of the Al base beam without the attachment of samples were either cut or clamped 1 cm at a time until the clamp was next to the sample. The unclamped side was then made to vibrate and the damping ratio was determined and the results were compared.

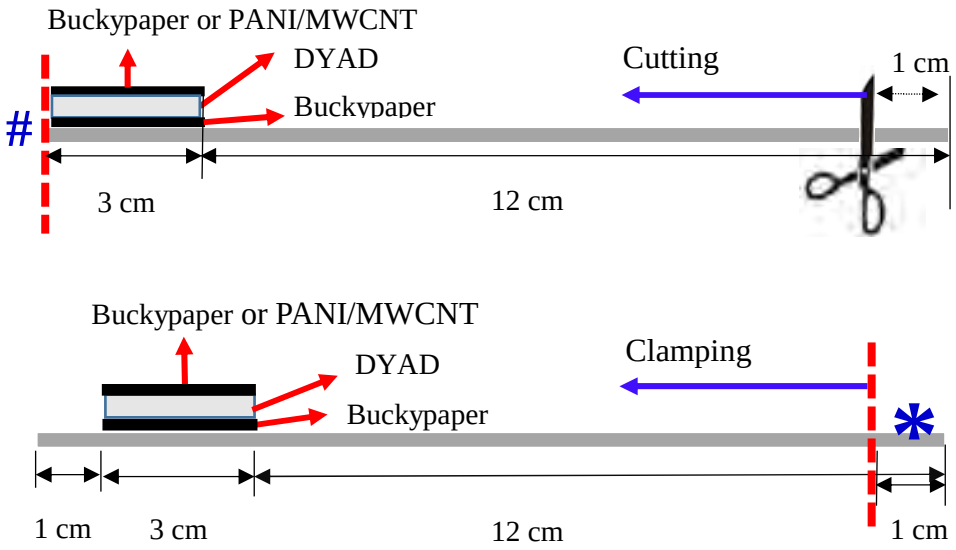

Figure 23. Schematic images of single sided attachment. The dimension of samples, Al beams and the locations where samples were attached; the locations of sample side, #, and free end side, *, where the beam was clamped; and the directions and lengths for both beam removal and clamping.

Double sides' attachment mode of Buckypaper/DYAD/ (PANI/MWCNT) and Buckypaper/DYAD/Buckypaper nanocomposites films

All the dimensions of sample and aluminum base beams, the clamped locations and the

directions and lengths for both cutting and clamping are kept the same as the second single side attachment mode described above. The only change that was made was that the aluminum base was covered on both sides by the sample (See **Fig. 24**). Also, the free vibration test of double sides' attachment of Buckypaper/DYAD alone was studied as the control group for both Buckypaper/DYAD/ (PANI/MWCNT) and Buckypaper/DYAD/Buckypaper nanocomposites films systems.

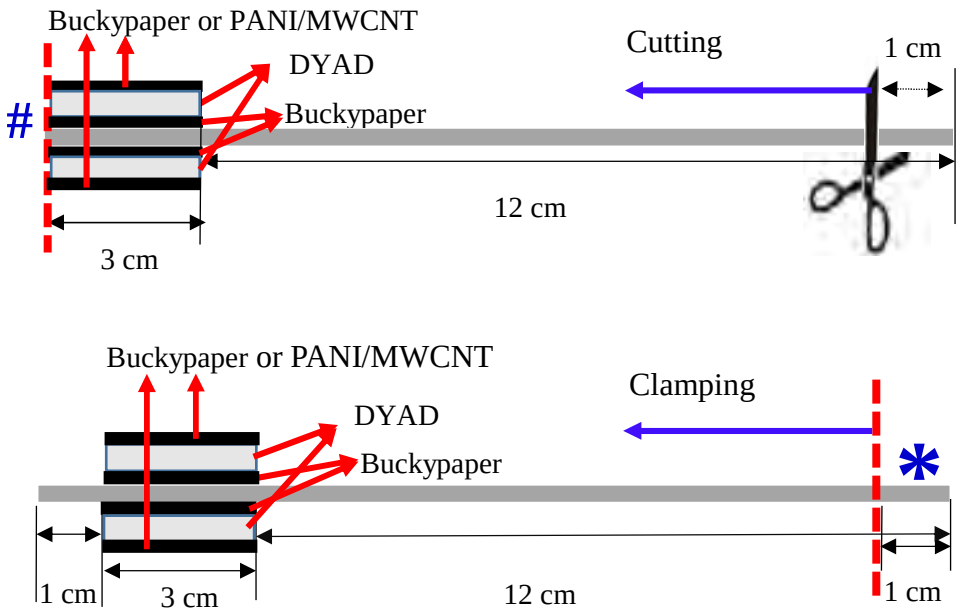

Figure 24. Schematic images of double sided attachment. The dimension of samples, Al beams and the locations where samples were attached, the locations of sample side, #, and free end side, *, where the beam was clamped and the directions and lengths for both beam removal and clamping.

Damping Test Methodology

The cantilever beams of **Figs. 23** and **24** were given small initial displacement and then released for free vibration. Free end displacements were measured by a laser vibrometer and a two channels digital oscilloscope was used display and store the signal. Five trials were made for each setup and the mean value of the damping ratio was calculated. This ratio can be related to the logarithmic decrement of consecutive maxima of end displacements and can be correlated to how much vibration energy is removed from the sample. The higher the damping ratio, the better the sample acts as a damper.

Results and Discussion

Damping ratios of single side's attachment of Buckypaper/DYAD, Buckypaper/DYAD/ (PANI/MWCNT) and Buckypaper/DYAD/Buckypaper nanocomposites films

The composite system is built in this manner for a reason. The first layer of Buckypaper has been found to be a very good and sensitive strain sensor and should be placed closest to the beam. The second layer of DYAD has been shown to be a very good viscoelastic material for damping purposes but its main feature is energy removal through shear. The DYAD cannot function without

a constraining layer. Here we add either another layer of PANI/MWCNT or Buckypaper. Both have better characteristics than the constraining layer used in Levy and Chen [12, 14] being stronger and cheaper to manufacture (PANI/MWCNT) or stronger and lighter (Buckypaper) in the other case. Also in the PANI/MWCNT case, it can contribute to damping compared to just Buckypaper.

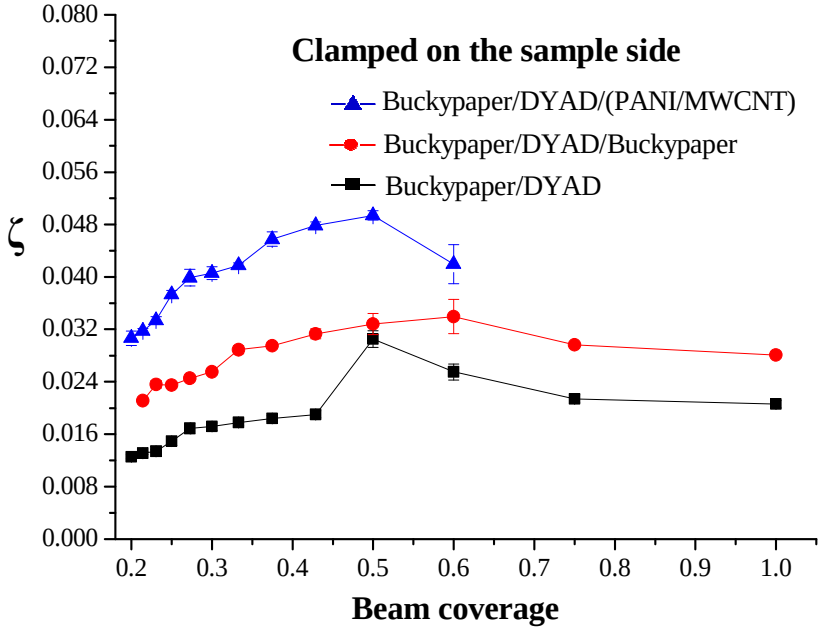

Figure 25. Damping ratios comparison of both sides attached Buckypaper/DYAD/ (PANI/MWCNT), Buckypaper/DYAD and Buckypaper/DYAD/Buckypaper when clamped on the sample side, #.

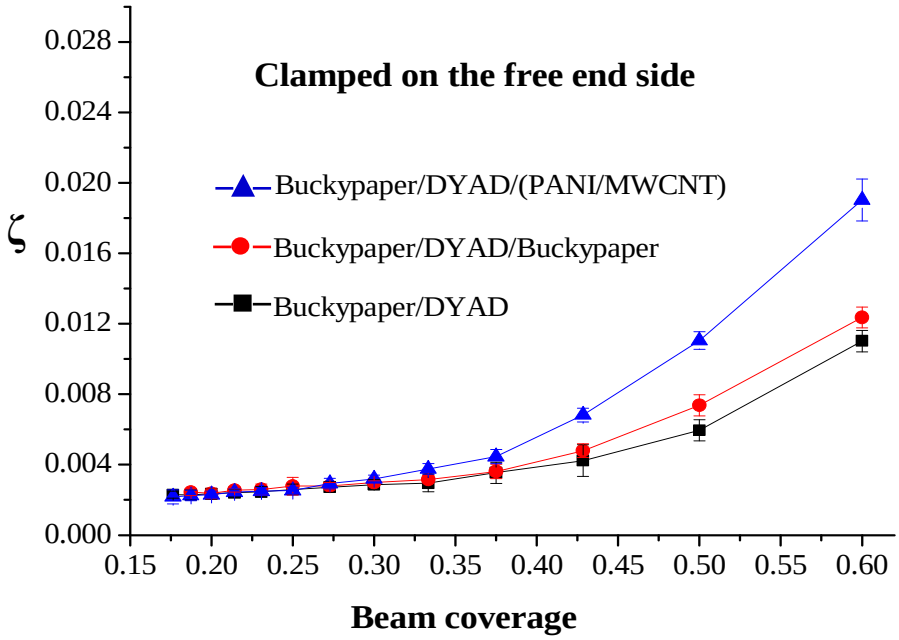

Figure 26. Damping ratios comparison of both sides attached Buckypaper/DYAD/ (PANI/MWCNT), Buckypaper/DYAD and Buckypaper/DYAD/Buckypaper when clamped on the free end side, *.

Herein, both **Figs. 25 and 26** bore out these trends. Compared with Buckypaper/DYAD alone, the damping ratios are higher in either case, i.e., with Buckypaper or PANI/MWCNT upon it as a

constrained layer for both clamped on the sample side and clamped on the free end side. Furthermore, Buckypaper/DYAD/ (PANI/MWCNT) system has higher damping ratios than that of the Buckypaper/DYAD/Buckpaper composite. One of the reasons is PANI/MWCNT weighs more than Buckypaper. However, as PANI is one of the cheapest polymers and PANI/MWCNT is very easy to synthesize. Also, PANI/MWCNT has some unique properties, such as thermal-electric properties. So, it's meaningful for PANI/MWCNT to be a constrained layer.

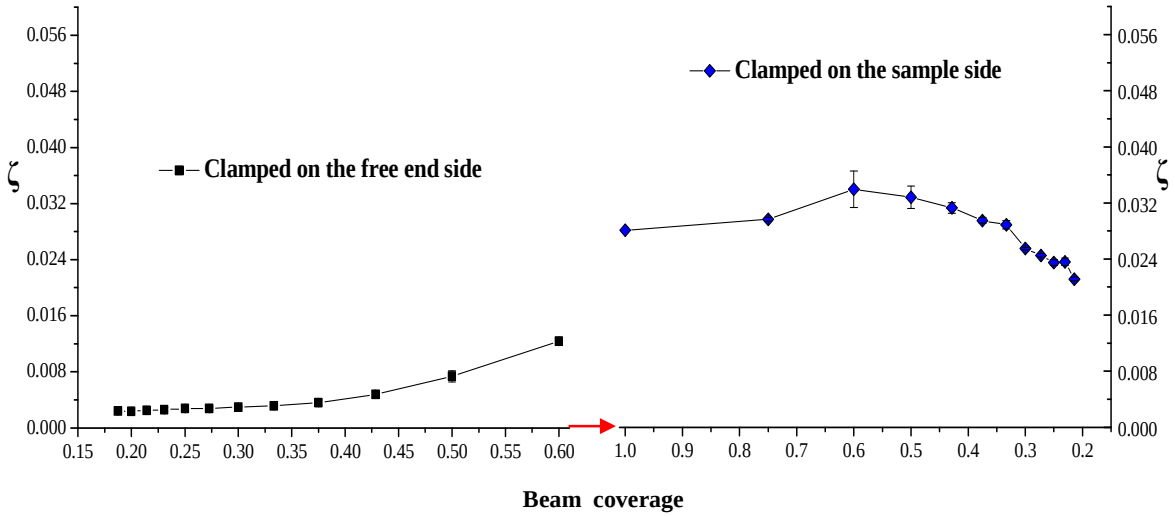

Figure 27. Damping ratios of double sides attached Buckypaper/DYAD/buckypaper clamped on the free end side, *, and the sample side, #.

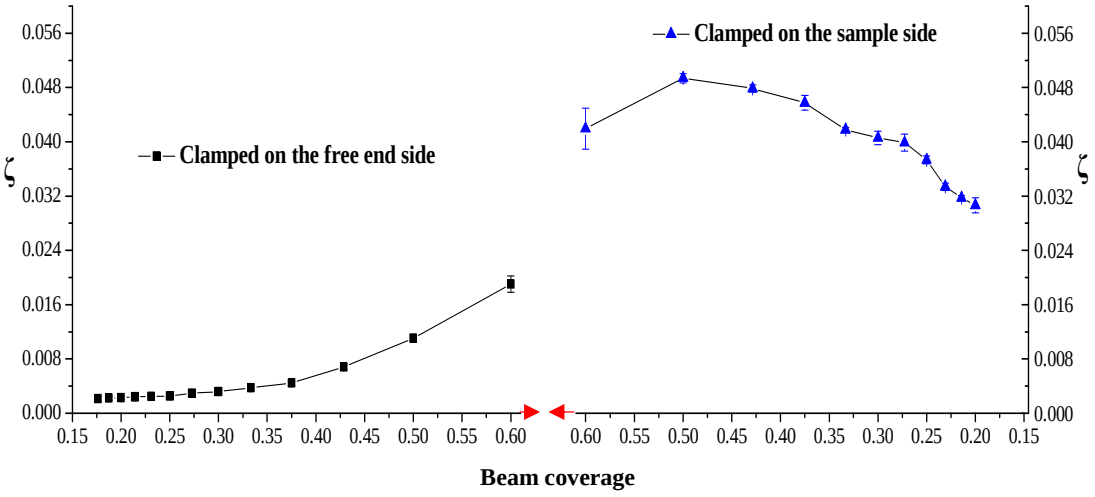

Figure 28. Damping ratios of double sides attached Buckypaper/DYAD/(PANI/MWCNT) clamped on the free end side, *, and the sample side, #.

Figures 27 and **28** provide comparisons of the damping ratio for the two combinations being evaluated. As can be seen the double side attachment of Buckypaper/DYAD/(PANI/MWCNT) provides better damping by close to 60% when clamped on the sample side irrespective of coverage. One the free end side, the increase in damping depends on the amount of coverage, reaching about 50% at half beam coverage. The trends follow those seen in Levy and Chen [6, 7].

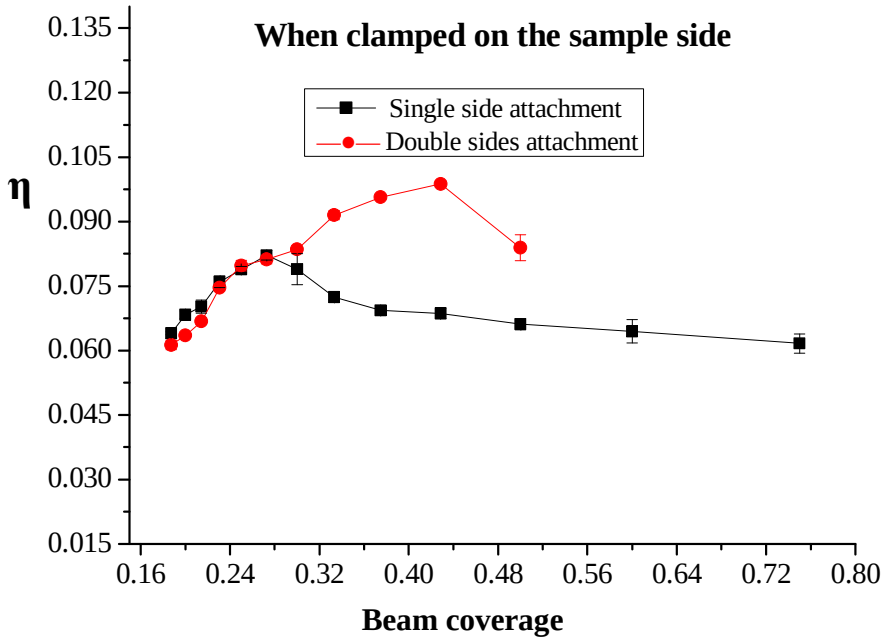

Figure 29. Comparison between single side and double sided attachment of the Buckypaper/DYAD/ (PANI/MWCNT) sample when clamping on the sample side, #.

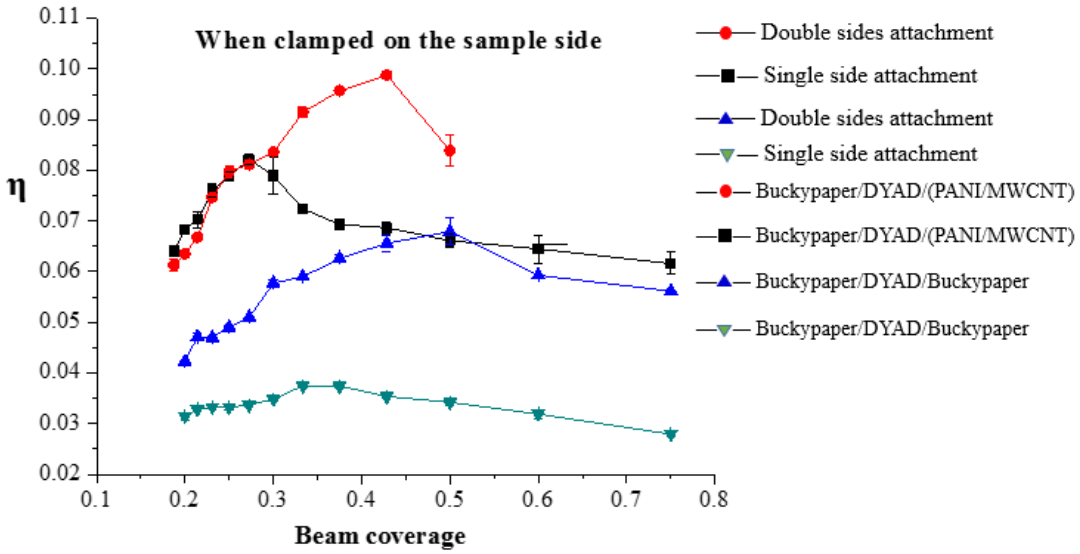

Figure 30. Comparison of single side and double sided attachment of both Buckypaper/DYAD/Buckypaper and Buckypaper/DYAD/ (PANI/MWCNT) sample for both clamping conditions

Figures 29 and **30** provide a comparison of the loss factor of the Buckypaper/DYAD/ (PANI/MWCNT) for single side and double side attachment as a function of beam coverage. Loss factor is twice the damping ratio for damping ratios less than 0.3 [5]. In **Fig. 29** we note that for this system the double sided coverage provides increased damping by 50% at a 40% beam coverage when clamped on the sample side than the single side. In **Fig. 30** single side versus double side attachment are compared for the two composite systems. We note that the PANI/MWCNT "constraining layer" does a much better job in either single or double side attachment.

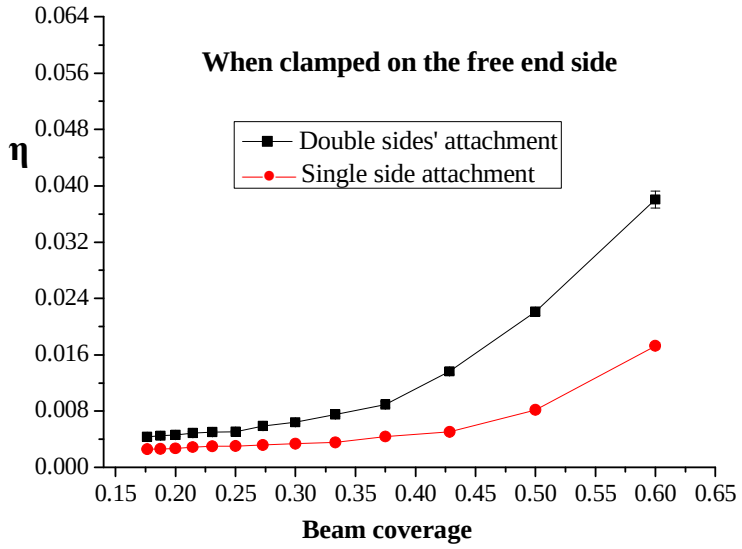

Figure 31. Comparison between single side and double sided attachment of the Buckypaper/DYAD/ (PANI/MWCNT) sample when clamping on the free end side, *.

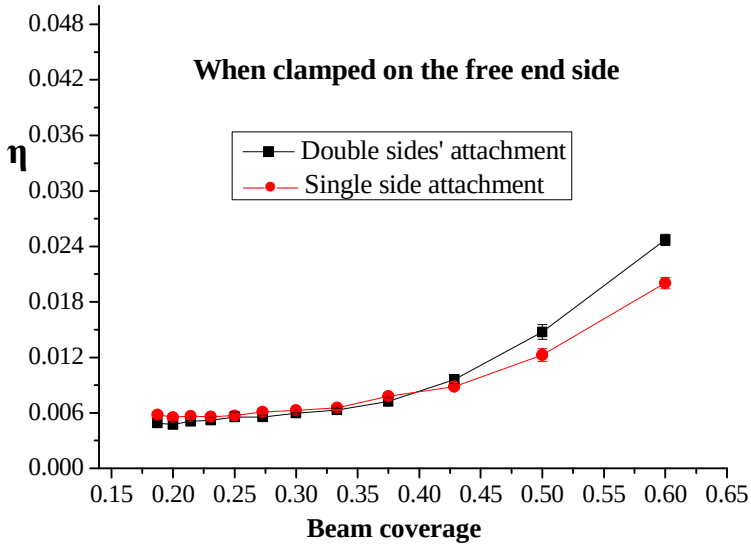

Figure 32. Comparison between single side and double sided attachment of the Buckypaper/DYAD/ Buckypaper sample when clamping on the free end side, *.

Finally in **Figs. 31** and **32** we present the loss factors for both systems when clamped on the free end side. We not that the loss factors are much smaller than when clamped on the sample side. Yet the loss factor increases with increasing coverage. We do note that at low beam coverage, the Buckypaper "constraining layer" provides equal (double sided) or better (single sided) loss factor than the PANI/MWCNT "constraining layer" composite. This is due to the PANI/MWCNT being heavier and acting more like an end mass than the Buckypaper composite.

Conclusions regarding these two Buckypaper/DYAD/ constraining layer systems

These two systems were considered to take advantage of some inherent strengths: either less expensive production or stronger constraining layer than the previous steel constraining layer used in [6, 7].

- In comparison to the steel constraining layer, both the PANI/MWCNT and the Buckypaper are less heavy.
- The PANI/MWCNT constraining layer system produced higher loss factors than the Buckypaper constraining system or a system with no constraining layer (no third layer).
- There was a clear coverage length at which the loss factor was a maximum and for the systems tested the maxima occurred at around the 30-40% beam coverage length.
- Loss factors for the sample side clamping was much better than the free end clamping system.

Conclusions Based Upon Results Obtained to Date

In reviewing the results obtained to date regarding damping and placement of the damping strain sensor-damping patch we find that:

- Damping in increased by placing the sensor patch at the fixed end of the cantilever beam. This has not changed with respect to existing results. However, when a sensor patch is place on one side of the beam only, a larger sized patch is required to obtain any sizable damping effect.
- Damping increases as the sensor patch length covers more of the beam and there appears to be an optimum length of the sensor patch that produces the best damping.
- Damping increases as the sensor patch covers more of the width of the beam.
- Adding too much PANI to the sensor patch destroys the linear sensing capability of the sensor patch. Those the load strain diagram appears to be nonlinear, we have found that in the 3 distinct regions found the stress-strain behavior remains linear with virtually the same slope within the accuracy of our instruments.
- Creating a composite produces better damping capabilities for the sensor patch than just MWCNT buckypaper sensor patches.
- Because of the character of the MWCNT, we see the same repeatability behavior in the composite PANI/11% MWCNT
- Other sensor composite systems have been revisited as they show promise of higher damping, but that may be tempered by their nonlinear behavior as sensors or by weight factors which can affect the operation of the system.

Part II Continuing Work

Though the grant has come to an end, there are several items that were not completed that we plan to finish and to report to the agency, if allowed, once those items are completed.

Temperature impact study

Some references [3, 6, 7, 15] stated that the temperature will affect specimen strain sensor performance and that was one of the reasons the sensor is covered by the layers of adhesive to isolate it from the environment. Therefore, the next step is to study the temperature change on the sample. The temperature range will be chosen 0 ^{0}C to 100 ^{0}C, to simulate conditions from freezing to close to boiling temperature. We have not been able to come up with a viable idea of how to test this in some repeatable fashion. We have created an apparatus that can test the beam and sensor together but as of now the temperature can be lowered to approximately 18 ^{0}C but is not easily repeatable. We plan to revisit this aspect.

Damping property and strain sensor properties of the PU/ZnO/MWCNT films, PU/ZnO films

We have already gotten some damping tests results for the composite PU-ZnO-MWCNT. Next step

will be that more tests will be done to get more results of those composites.

Evaluation of the control problem with the Sensor

The control of the beam needs to be evaluated using the sensor to see if it achieves one of the goals of the project. This will require addition of Shape Memory Alloy (SMA) and using heaters as we have done in the past. Here we provide the gist of what we are planning to do as a continuation of the work

Sandwich Structure Modeling

For the purposes of discussion, an Euler-Bernoulli cantilever beam fully covered with MWCNT composite as strain sensor and free layer damping treatment on its top and SMA layer as actuator on its bottom will be adopted to illustrate the new configuration, as shown in the figure below. The multifunctional MWCNT layer here is the PANI/MWCNT sensor. The mathematical model of the system is developed based on the following assumptions of a single layer:

1. the beam deflection is small and the beam has uniform across section;
2. the beam is isotropic and homogenous;
3. the bonding layers are perfect, there is no slip, no overlap and no gap across the interface;
4. the temperature effect will be considered using experimental data;
5. the rotatory inertia in all layers are considered negligible and neglected; and,
6. the longitudinal effect and the axial force effect are neglected.

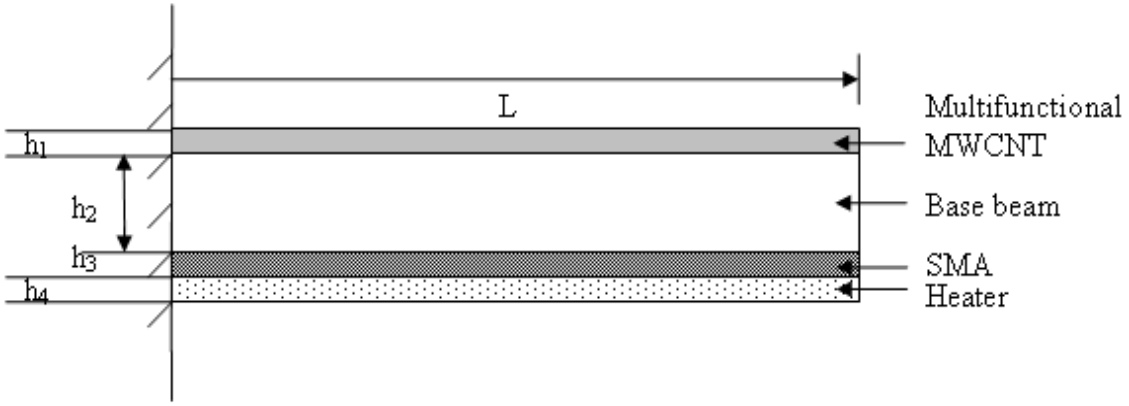

Figure 33: Cantilever beam with MWCNT multifunctional treatment

Similar to the analysis in [15, 16], the non-dimensional governing equation of the multifunctional treated cantilever beam can be found as:

$$\{\frac{1}{12}\bar{H}_2^{\,3}+\frac{1}{12}\bar{E}_1\bar{H}_1^{\,3}-\frac{\bar{H}_2^{\,2}[\bar{H}_1+\bar{H}_2]}{4}+\frac{[2\bar{E}_1\bar{H}_1\bar{H}_2+\bar{E}_1\bar{H}_1^2+\bar{H}_2^{\,2}]}{2[\bar{E}_1\bar{H}_1+\bar{H}_2+\bar{E}_3\bar{H}_3+\bar{E}_4\bar{H}_4]}\times$$

$$[\bar{H}_2(\frac{\bar{H}_1+\bar{H}_2}{2})+\bar{E}_3\bar{H}_3(\frac{\bar{H}_1+2\bar{H}_2+\bar{H}_3}{2})+\bar{E}_4\bar{H}_4(\frac{\bar{H}_1+2\bar{H}_2+2\bar{H}_3+\bar{H}_4}{2})]\}\frac{\partial^4\bar{w}}{\partial\bar{x}^4}+\frac{\partial^2\bar{w}}{\partial\bar{t}^2}$$

$$=-\frac{(2\bar{E}_1\bar{H}_1\bar{H}_2+\bar{E}_1\bar{H}_1^2+\bar{H}_2^2)\bar{H}_3}{2[\bar{E}_1\bar{H}_1+\bar{H}_2+\bar{E}_3\bar{H}_3+\bar{E}_4\bar{H}_4]}\bar{\sigma}_r[\delta'(\bar{x})-\delta'(\bar{x}-1)] \qquad (6)$$

Where:

$$\bar{x}=\frac{x}{L},\quad \bar{t}=\frac{t}{t_0},\bar{w}=\frac{w}{L},\bar{H}_1=\frac{h_1}{L},\bar{H}_1=\frac{h_1}{L},\bar{H}_2=\frac{h_2}{L},$$

$$\bar{H}_3=\frac{h_3}{L},\bar{H}_4=\frac{h_4}{L},\quad \bar{E}_1=\frac{E_1^*}{E_2}=\frac{E_1(1+j\eta_1)}{E_2}=\frac{E_1}{E_2}(1+j\eta_1)$$

$$\bar{E}_3=\frac{E_s^*}{E_2},\bar{E}_4=\frac{E_4}{E_2},\bar{\sigma}=\frac{\sigma_r^*}{E_2},t_0^2=\frac{mL}{E_2 b} \tag{7}$$

Boundary conditions are:

$$\bar{x}=0:\quad \bar{w}=0,\ \frac{\partial\bar{w}}{\partial\bar{x}}=0 \tag{8}$$

$$\bar{x}=1:\quad \frac{\partial^2\bar{w}}{\partial\bar{x}^2}=0\ ,\ \frac{\partial^3\bar{w}}{\partial\bar{x}^3}=0 \tag{9}$$

in all the foregoing equations, $\bar{w}$ is the non-dimensional transverse displacement, E_i is the Young's modulus of the i^{th} layer, E_s^* is the Young's modulus of the SMA material, and σ_r^* is the recovery stress of the SMA material.

By changing the SMA layer temperature, the elastic modulus of the SMA layer will change, which means the coefficient of the differential equation (7) will change correspondingly and this will result in the alteration of the system natural frequency. At the same time, the temperature change will introduce an SMA recovery stress, which is the term on the right side of Equation (7), and, is actually the control input.

Frequency Factor and Loss Factor

When one considers the Bernoulli-Euler model one can obtain a variable-separable solution. That is:

$$\bar{w}=\bar{w}_1 e^{j\Omega^*\bar{t}}e^{\lambda\bar{x}} \tag{10}$$

where λ and Ω^* are unknown characteristic values and complex natural frequencies, respectively. The complex natural frequency Ω^*, the associated real frequency ω_n, and the composite system loss factor, η_{sys} are related by [15]:

$$\Omega_n^2=\omega_n^2(1+j\eta_{sys}) \tag{11}$$

$$\omega_n=real(\Omega_n^*) \tag{12}$$

$$\eta_{sys}=\frac{\mathrm{Im}(\Omega^{*2})}{\mathrm{Re}(\Omega^{*2})} \tag{13}$$

Figure 34 shows results that were obtained previously for the system loss factor as a function of just the Buckypaper multifunctional damping layer thickness and its Young's modulus. These results were consistent with previous analyses of similar system [17, 18]. We expect to get results similar to these when we complete the numerical simulation based upon our different sensor material parameters. When thickness ratio h_1/h_2 (sample/base beam) is larger than 2, system loss factor starts to decrease and gradually approaches a constant with increase of the free layer damping layer thickness. This is because the high Young's modulus damping material not only provides damping effect, but also increases the system stiffness at the same time, which in turn usually reduces the damping effect. This analysis indicates that there exists a maximum for application of hard damping materials to achieve the best damping effect. However, since our Young's modulus ratio is greater than one there appears to be a contradicting effect that the system loss factor continues to increase. This will also be investigated.

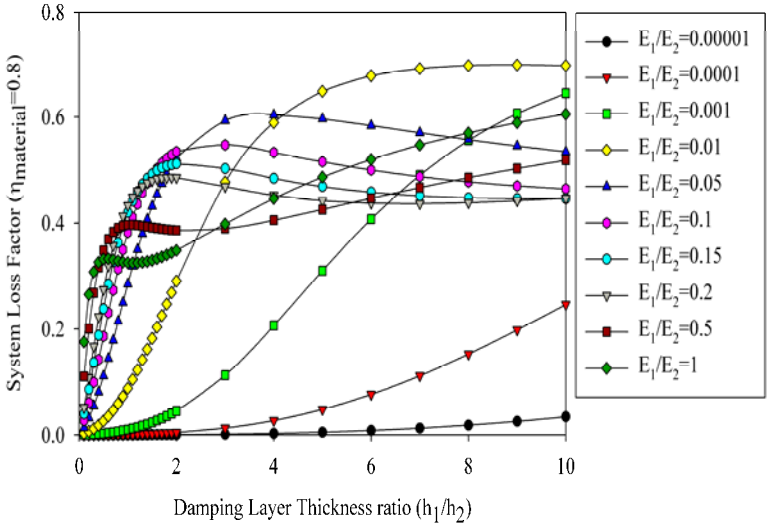

Fig. 34: System loss factor vs. damping layer property ($\eta_{material}$ =0.8)

Modal Solution of Governing Equation

For active control of the cantilever beam vibration, we need to solve the governing equation with external input such as the recovery stress of SMA, and the system properties change due to the temperature effect. Again, the governing equation for an Euler-Bernoulli beam transverse vibration can be solved by separation of variables. For cantilever boundary conditions, assume the variable separable solution as:

$$\overline{w}(\overline{x},\overline{t}) = \sum_{i=1}^{\infty} \Phi_i(\overline{x}) T_i(\overline{t}) \tag{14}$$

$$\Phi_i(\overline{x}) = [\sin(\beta_i \overline{x}) - \sinh(\beta_i \overline{x})] - \alpha_i [\cos(\beta_i \overline{x}) - \cosh(\beta_i \overline{x})] \tag{15}$$

α_i and β_i are determined by:

$$\cos(\beta_i) * \cosh(\beta_i) = -1 \tag{16}$$

$$\alpha_i = \frac{\sin\beta_i + \sinh\beta_i}{\cos\beta_i + \cosh\beta_i} \tag{17}$$

By substituting Equations (14) and (15) into the governing Equation (6), applying the orthogonal property and integrating over the beam length, we then have the unknown $T_i(t)$ as function of the external control input:

$$\ddot{T}_i(\bar{t}) + A_i(\bar{t})T_i(\bar{t}) = B_i u(\bar{t}) \tag{18}$$

Where:

$$A_i(\bar{t}) = \{\frac{1}{12}\bar{H}_2^{\,3} + \frac{1}{12}\bar{E}_1\bar{H}_1^{\,3} - \frac{\bar{H}_2^{\,2}(\bar{H}_1+\bar{H}_2)}{4} + \frac{(2\bar{E}_1\bar{H}_1\bar{H}_2 + \bar{E}_1\bar{H}_1^2 + \bar{H}_2^{\,2})}{2(\bar{E}_1\bar{H}_1 + \bar{H}_2 + \bar{E}_3\bar{H}_3 + \bar{E}_4\bar{H}_4)} \times$$
$$[\bar{H}_2(\frac{\bar{H}_1+\bar{H}_2}{2}) + \bar{E}_3\bar{H}_3(\frac{\bar{H}_1+2\bar{H}_2+\bar{H}_3}{2}) + \bar{E}_4\bar{H}_4(\frac{\bar{H}_1+2\bar{H}_2+2\bar{H}_3+\bar{H}_4}{2})]\}\beta_i^4 \tag{19}$$

$$B_i = -\frac{[\Phi_i'(\bar{x}=1) - \Phi_i(\bar{x}=1)]}{\Lambda_i} \tag{20}$$

$$u(\bar{t}) = \frac{(2\bar{E}_1\bar{H}_1\bar{H}_2 + \bar{E}_1\bar{H}_1^2 + \bar{H}_2^2)\bar{H}_3}{2[\bar{E}_1\bar{H}_1 + \bar{H}_2 + \bar{E}_3\bar{H}_3 + \bar{E}_4\bar{H}_4]}\bar{\sigma}_r \tag{21}$$

$$\Lambda_i = \int_0^1 \Phi_i^2(\bar{x})d\bar{x} \tag{22}$$

These equations will be evaluated using the different sensor material properties in our investigation of the control of the sensor and SMA actuator system. Also, depending on the ease of solutions and results, we will also endeavor to evaluate what we find for the Timoshenko beam, model as well. We have the materials and also expect to begin the testing by the end of this month. We expect to obtain good results in the near future.

Thank you

We would like to thank the ARO for giving us the opportunity to carry out this research. Your funding support was very much appreciated and has helped several students achieve their educational goals. Without your help it would have been much harder.

References

[1] Johnson, C.D., Design of passive damping system. Journal of mechanical Design, Transactions of the ASME 1995; 117B: 171-176.

[2] Li, X. and Levy, C., Multi-walled carbon nanotube film as strain sensors for structural vibration control, NSTI conference, Santa Clara, California, May 21-24, 2007. Technical Proceedings of the 2007 NSTI Nanotechnology Conference and Trade Show, 2007, Vol 3,256-259

[3] Li, X., Levy, C. and Elaadil, L. Multiwalled Carbon Nanotube Film for Strain Sensing, Institute of Physics' Journal–Nanotechnology, 2008; 19:045501, 7pp Ref: NANO/252812/PAP/170180 .

[4] Lin W., Kong X., Levy, C. Preparation of Polyaniline Multi-wall carbon nanotubes nanocomposites films/discs and characterization of their electrical, mechanical and damping properties. Sensors and Transducers 2015; 187(4):129-137.

[5] Rao SS. Mechanical Vibrations, 4th Edition, Pearson-Prentice Hall, 2004; p 150 and p 686.

[6] Chen Q, Levy C. Vibration Analysis of a Partially Covered, Double Sandwich Cantilever Beam with Concentrated Mass at the Free End. International Journal of Solids and Structures 1994; 31: 2377-2391.

[7] Chen Q, Levy C. Vibration Characteristics of a Partially Covered Double Sandwich Cantilever Beam. AIAA Journal 1996; 34: 2622-2626.

[8] Lin W, Rotenberg Y, Ward KP, Fekrmandi H, Levy C. Multifunctional Materials of Polyurethane/MWCNT and Evaluation of Damping and Displacement Sensing Properties. Submitted to Journal of Nanomaterials.

[9] Sasikumar K, Manoj NR, Ramesh R, Mukundan T. Carbon nanotube-polyurethane nanocomposites for structural vibration damping. Int J Nanotechnol 2012;9:1061–71. doi:10.1504/IJNT.2012.049467.

[10] Li L, Tian B, Zheng Y, Wang Y, Chen F, Tong Y, et al. Method for preparing NiTi spring-carbon nanotube-polyurethane composite damping materials. 2014.

[11] Li X, Levy C. A Novel Strain Gauge with Damping Capability. Sensors and Transducers Journal, Special Issue-MEMS: from Micro Devices to Wireless Systems 7 (10), pp. 5-14 (2009). Also, http://www.sensorsportal.com/HTML/DIGEST/P_SI_79.htm

[12] Li X, Levy C, Agarwal A, Datye A, Elaadil L, Keshri AK, Li M. Multifunctional carbon nanotube film composite for structure health monitoring and damping. The Open Construction and Building Technology Journal 2009; 3: 146-152.

[13] Soyoz S, Feng MQ. Instantaneous damage detection of bridge structures and experimental verification. Structural Control and Health Monitoring 2008; 15(7): 958-973.

[14] Kai HH, Marvin WH, Paul JB. Overview of vibrational structural health monitoring with representative case studies. Journal of Bridge Engineering 2006; 11(6): 707-715.

[15] Chen Q, and Levy C. Active vibration control of elastic beam by means of shape memory alloy layers, Smart Materials and Structures, 1996; **5** (4): 400-406.

[16] Chen Q, and Levy C. Vibration Control of Flexible Beam by Using Smart Damping Structures, Composites-Part B. Engineering, 1999; **30**:395-406.

[17] Ravi, S. S. A., Kundra, T. K. and Nakra B. C., 1995, "A response re-analysis of damped beams using eigenparameter perturbation", Journal of Sound and Vibration, **179 (3)**, pp. 399-412.

[18] Torvik, P. J., 2007, "Analysis of free-layer damping coating", Key Engineering Materials, **33**, pp.195-214.

Part III - Students and Research Associate being supported on the grant:

Students supported:

- Ayobami Bamgbade, PhD student. Supported Fall 2014, Spring 2015. 3rd year PhD student. passed his qualifiers. Grad GPA: 3.41
- Melissa Morris, PhD student. Supported Fall 2014 and Spring 2015. She is presently working on her dissertation. Grad GPA: 4.00
- Yonatan Rotenberg, BS student, worked on dynamic testing, drift tests, vibration tests, static and dynamic sensing. Graduated Fall 2014. Undergraduate GPA: 3.75
- Kevin Ward-Jimenez, BS student, worked on dynamic testing, drift tests, vibration tests, static and dynamic sensing. Undergraduate GPA: 3.23

Post-Doctoral Research Associate supported:

- None at the present.

Other students working on grant:
Other students working on the grant but <u>not</u> supported from the grant, but supported by the Mechanical and Materials Department:

- Weiwei Lin, PhD student, is working on the chemistry of creating the different sensors. She has worked on the vibration testing, dynamics and static testing of the sensors, drift tests. Grad GPA: 3.61.
- Hadi Fekrmandi, PhD student, worked on the laser vibrometer tests and the code to convert the data to usable information. Grad GPA: 3.86

Papers Generated Under the Grant's Auspices:

-Melissa Morris, Sabri Tosunoglu, "Robotic Ocular Surgery," Proceedings of the 28th Florida Conference on Recent Advances in Robotics, FCRAR 2015, Melbourne, Florida, May 14-15, 2015.

-Jonathan Hipps, Alejandro Osorio, Gianfranco Pisani, Sebastian Rojas, Melissa Morris, Sabri Tosunoglu, "Laser Eye Surgery Robot," Proceedings of the 28th Florida Conference on Recent Advances in Robotics, FCRAR 2015, Melbourne, Florida, May 14-15, 2015.

-Danilo Delgado, Michael Fisher, Lucia Melara, Melissa Morris, Sabri Tosunoglu, "SWAT Bot and its Future Use as a Strategic Response Robot," Proceedings of the 28th Florida Conference on Recent Advances in Robotics, FCRAR 2015, Melbourne, Florida, May 14-15, 2015.

-Alexis Garo, Lucia Melara, Robert Scott, Melissa Morris, Sabri Tosunoglu, "Natural Gait Inducing Transtibial Prosthetic," Proceedings of the 28th Florida Conference on Recent Advances in Robotics, FCRAR 2015, Melbourne, Florida, May 14-15, 2015.

-Fekrmandi, H., Rojas, J., Tansel, I. N., Yapici, A., & Uragun, B. (2015). Investigation of the computational efficiency and validity of the surface response to excitation method. Measurement, 62, 33-40.
-Fekrmandi, Hadi, et al. "Inspection of the Integrity of a Multi-Bolt Robotic Arm Using a Scanning Laser Vibrometer and Implementing the Surface Response to Excitation Method (SuRE)." International Journal of Prognostics and Health Management 5.1 (2014): 1-10.
-Fekrmandi, H., Tansel, I.N., "Laser Scanning Vibrometer for Remote Process Performance Monitoring of Automated Manufacturing Operations", ASME Early Career Technical Conference Proceedings, ECTC 2014, Vol. 13, pages 55-60.
-Fekrmandi, H., Tansel, I.N., Oyola, K., Alsenawi, A. "A non-contact method for part-based process performance monitoring in end milling operations", International Journal of Advanced Manufacturing Technology, Springer Publications. DOI 10.1007/s00170-015-7523-2
-Fekrmandi, H., Ramanathan, G., Tansel, I.N., "Automation of manufacturing process monitoring for CNC milling machines using a remote sensing method based on high–frequency surface guided waves", 27th Florida Conference on Recent Advances in Robotics, FCRAR 2014, May 8-9, Florida International University, Miami, Florida.
-Lin W., Kong X., Levy, C. Preparation of Polyaniline Multi-wall carbon nanotubes nanocomposites films/discs and characterization of their electrical, mechanical and damping properties. Sensors and Transducers 2015; 187(4):129-137.
-Lin W, Rotenberg Y, Ward KP, Fekrmandi H, Levy C. Multifunctional Materials of Polyurethane/MWCNT and Evaluation of Damping and Displacement Sensing Properties. Submitted to Journal of Nanomaterials.

Part IV. Equipment bought on the grant in Years 1-4.

Polytec VibraScan PSV-400-B laser Doppler vibrometer system. The system measures vibration amplitudes up to +/- 10 m/s and acquires data up to 40kHz over two channels. It can scan a grid of 256X256 point density and optional software extension to 512 x 512 for surface vibration measurements.

LeCroy ArbStudio 1102/2ch 16bit 1GS/s Arbitrary Waveform Generator.

Spectrum analyzer made up of the following:

- 1 VIBPOINT-DT9837A USB VIBpoint Precision Measurement System For Sound and Vibration Analysis
- 1 DT9832A-02-2-BNC Simultaneous USB Data Acquisition (DAQ) Module; 16-bit, 2.0MHz per channel, 2 AI, 2 AO, 32 DIO, 2 C/T, 3 Q/D, BNC connectors
- Software and security key to run the analyzer
- New VTS 65 vibration shaker apparatus had to be bought as our current VTS50 failed during one of the tests related to the project

United Data Technologies Laptop computer to run the spectrum analyzer software

Gamry Instruments Potentiostat and HP Compac 8300 computer system with ancillary equipment for measurement of certain material properties.

Chemicals, glass equipment, homogenizer, hydrothermal chemical reactors all required to produce the MWCNT/PU/ZnO composite sensor layer for testing as part of the proposal. We also bought protective gloves, lab coat as part of protective equipment for graduate student working in the lab.

All vibrometer and related equipment are being used to support courses such as System Dynamics, System Indentification and Machine Intelligence, Introduction to Mechatronics, Advanced Vibrational Analysis.

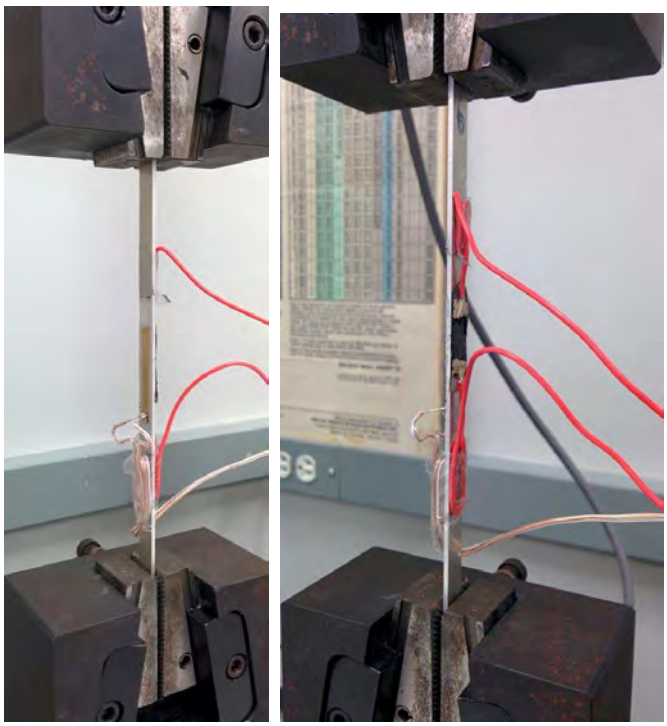

Same beam with strain gage showing and with sensor showing, both in loading mode

Wheatstone Bridge setup for load sensing

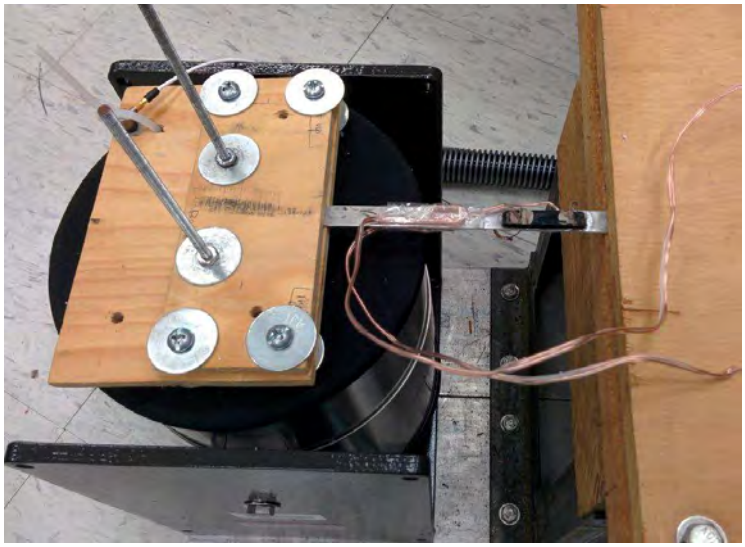

Beam and Sensor in dynamic testing mode.

Beam and sensor being interrogated by the laser vibrometer.

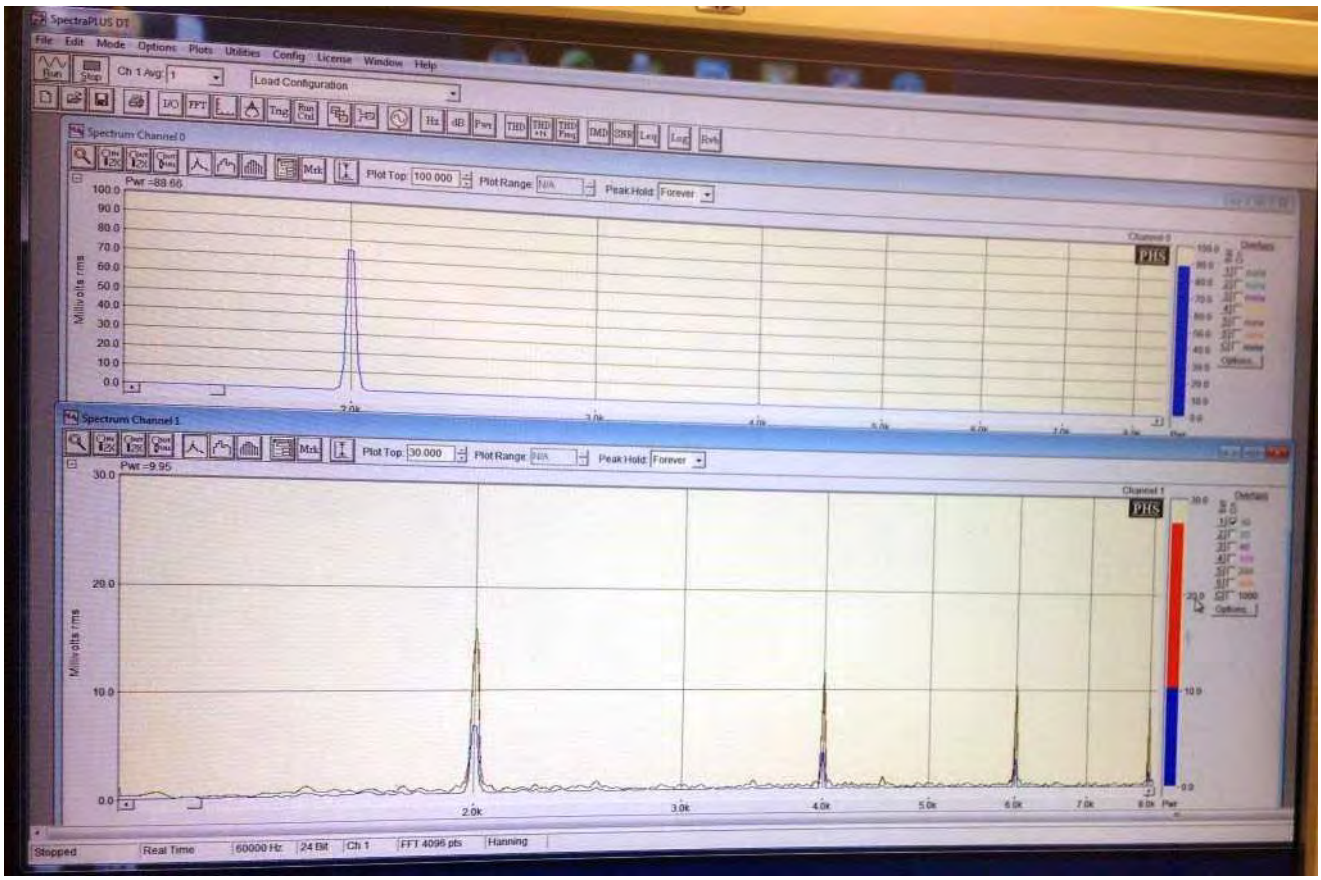

SpectralPLUS DT output from dynamic tests.